Exclusive and dissociative J/ψ photoproduction, and exclusive dimuon production, in p-Pb collisions at $\sqrt{s_{\rm NN}} = 8.16$ TeV

S. Acharya *et al.*[*]
(ALICE Collaboration)

(Received 10 May 2023; accepted 12 October 2023; published 13 December 2023)

The ALICE Collaboration reports three measurements in ultraperipheral proton-lead collisions at forward rapidity. The exclusive two-photon process $\gamma\gamma \to \mu^+\mu^-$ and the exclusive photoproduction of J/ψ are studied. J/ψ photoproduction with proton dissociation is measured for the first time at a hadron collider. The cross section for the two-photon process of dimuons in the invariant mass range from 1 to 2.5 GeV/c^2 agrees with leading-order quantum electrodynamics calculations. The exclusive and dissociative cross sections for J/ψ photoproductions are measured for photon-proton center-of-mass energies from 27 to 57 GeV. They are in good agreement with HERA results.

DOI: 10.1103/PhysRevD.108.112004

I. INTRODUCTION

The strong electromagnetic fields present in ultraperipheral collisions (UPCs) offer a unique opportunity to study a variety of phenomena, such as photonuclear and two-photon processes [1–3]. These interactions are mediated by quasireal photons and characterized by an impact parameter larger than the sum of the radii of the colliding nuclei.

Two-photon interactions can give rise to exclusive nonresonant dimuon production. Precise measurements of this process can be used to test quantum electrodynamics (QED) calculations, such as light-by-light scattering [4,5] recently measured by ATLAS [6–8] and CMS [9], and higher-order QED effects [10]. The latter are expected to be sizable, since the photon couples to nuclei with a large coupling $Z\alpha$ where Z is the charge number and α is the fine structure constant [10]. Various theoretical calculations predict a different strength of higher-order effects in heavy-ion collisions [10–12]. The use of asymmetric p-Pb collisions may provide additional insight on higher-order corrections from multiphoton exchange with a single ion [1].

Measurements of cross sections of dilepton production using UPC samples, performed by ALICE in Pb-Pb [13] and p-Pb [14], CMS [15] and ATLAS [16] in Pb-Pb, and PHENIX [17] and STAR [18–20] in Au-Au, are consistent with leading-order (LO) QED calculations. However, latest precision measurements by ATLAS [21] revealed a significant discrepancy with LO QED predictions from the STARlight event generator [22], up to 20% at large rapidities. This discrepancy is discussed by the authors of the SuperChic event generator in Ref. [23]. They argue that STARlight does not take into account contributions from dilepton-nucleus impact parameters smaller than the nuclear radii, expected to be significant at high photon energies. Accounting for photons emitted at such impact parameters is also discussed in Refs. [10,24,25]. However, this effect alone does not allow the SuperChic authors to resolve the discrepancy with the ATLAS data [24]. The inclusion of higher-order corrections to the LO QED calculation could explain the ATLAS results, as suggested in Ref. [10]. Dilepton measurements were also performed in pp collisions by ATLAS [26,27] and CMS [28] and in $\mathrm{p\bar{p}}$ collisions by CDF [29,30]. These measurements did not explore the low invariant mass region at forward rapidities.

Dimuons can also be produced in photonuclear reactions, from the decay of a vector meson. In particular, dimuons can be produced from the decay of a J/ψ meson in the elastic process $\gamma + \mathrm{p} \to J/\psi + \mathrm{p}$ or with proton dissociation in the reaction $\gamma + \mathrm{p} \to J/\psi + \mathrm{p}^{(*)}$. The use of p-Pb collisions offers the possibility of assigning the photon to its source: the lead ion is in most of the cases the photon emitter due to its large charge number. The γp center-of-mass energy $W_{\gamma\mathrm{p}}$ is a function of the J/ψ rapidity: $W^2_{\gamma\mathrm{p}} = 2E_{\mathrm{p}}M_{J/\psi}\exp(-y)$, where $M_{J/\psi}$ is the J/ψ mass, y is the J/ψ rapidity measured in the laboratory frame with respect to the proton beam direction, and $E_{\mathrm{p}} = 6.5$ TeV is the proton beam energy, corresponding to a center-of-mass energy in the p-Pb system of $\sqrt{s_{\rm NN}} = 8.16$ TeV. The energy range studied is $27 < W_{\gamma\mathrm{p}} < 57$ GeV, which corresponds to a longitudinal momentum fraction of the participating partons, Bjorken-x scale, in the range $5 \times 10^{-3} < x < 2 \times 10^{-2}$, where the

[*]Full author list given at the end of the article.

conversion is performed as $x = (M_{J/\psi}/W_{\gamma p})^2$. This is a similar kinematic domain as studied at HERA [31].

Exclusive J/ψ photoproduction is sensitive to the gluon distribution in protons, since its cross section scales with the square of the gluon parton density function in the target proton, according to LO QCD calculations [32]. This picture may change at next-to-leading order (NLO) according to the recent studies in Ref. [33]. At high $W_{\gamma p}$, a reduction in the growth rate of the exclusive J/ψ photoproduction cross section would indicate that nonlinear QCD dynamics are present. These nonlinearities may arise from gluon recombination, which tame the growth of the gluon distribution, leading in the high-energy limit to the gluon saturation phenomenon [34].

On the other hand, J/ψ photoproduction off protons with proton dissociation is a scattering event that produces a J/ψ vector meson and, accompanied by a large rapidity gap, remnants of the dissociated proton. This process might serve as an experimental signature of subnucleonic fluctuations of initial state configurations in the proton target [35–37]. At high energies, the ratio of dissociative-to-exclusive cross sections is predicted to vanish, owing to the onset of gluon saturation at sufficiently small x [36,37].

At HERA, ZEUS and H1 have measured both the exclusive [38–40] and dissociative [40,41] J/ψ photoproduction off protons at γp center-of-mass energies ranging from 20 to 305 GeV. CDF has measured the exclusive process in $p\bar{p}$ collisions at $\sqrt{s} = 1.96$ TeV [30]. At the LHC, the exclusive process was studied in p-Pb at $\sqrt{s_{\rm NN}} = 5.02$ TeV by ALICE [14,42] and in pp at $\sqrt{s} = 7$ and $\sqrt{s} = 13$ TeV by LHCb [43–45]. The dissociative process has never been measured before at a hadron collider.

In this article, the measurement of exclusive dimuon continuum production in two-photon interactions in p-Pb UPCs at $\sqrt{s_{\rm NN}} = 8.16$ TeV is presented. It is performed in three intervals of dimuon invariant mass, in the range $1.0 < M_{\mu\mu} < 2.5$ GeV/c^2, and two intervals of rapidity, in the range $2.5 < y < 4.0$. The measurement of exclusive J/ψ photoproduction off protons is also presented along with the measurement of J/ψ photoproduction with proton dissociation. These three measurements are carried out in the forward rapidity region with respect to the proton beam direction, namely $2.5 < y < 4.0$, and at low dimuon transverse momentum, $p_{\rm T} < 3$ GeV/c. This corresponds to a range in the square of the momentum transferred at the proton vertex $|t| \lesssim 9$ GeV^2, where $t \approx -p_{\rm T}^2$.

II. EXPERIMENTAL SETUP AND TRIGGER

The ALICE detector is described in Ref. [46] and its performance is detailed in Ref. [47]. The main ALICE tracking detector used in this analysis is the single-arm muon spectrometer, covering the pseudorapidity interval $-4.0 < \eta < -2.5$.[1] The analysis also uses other detector systems, namely the silicon pixel detector (SPD), VZERO (V0), zero degree calorimeters (ZDCs), and ALICE diffractive (AD) detectors.

The muon spectrometer consists of a ten hadronic interaction length absorber, followed by five tracking stations, each made of two planes of cathode pad chambers. The third station is placed inside a dipole magnet with a 3 T × m integrated magnetic field. Muon tracks are reconstructed by the tracking algorithm described in Ref. [48] using the five tracking stations. The muon trigger system, downstream of the tracking chambers, consists of four planes of resistive plate chambers placed behind a 7.2 interaction length iron wall. The muon tracks detected in these planes are used in the trigger and matched off-line to the muon tracks reconstructed in the five tracking stations.

The central region $|\eta| < 1.4$ is covered by the SPD consisting of two cylindrical layers of silicon pixels, from which tracklets are reconstructed. Tracklets are track fragments created from the primary vertex and two reconstructed points in the SPD, one in each layer.

The V0 detector is composed of two arrays of scintillator counters, namely the V0C and V0A detectors. Each array consists of 32 cells forming four concentric rings with eight sectors each. V0C, placed at the longitudinal coordinate $z = -90$ cm, covers the interval $-3.7 < \eta < -1.7$, while V0A, $z = 330$ cm, covers the pseudorapidity interval $2.8 < \eta < 5.1$. The AD detector [49,50] is composed of two scintillator tile arrays, the ADC and ADA subdetectors, located at $z = -19.5$ and $z = +16.9$ m and covering the pseudorapidity ranges $-7.0 < \eta < -4.9$ and $4.7 < \eta < 6.3$, respectively. The time resolution of V0 and AD detectors is better than 1 ns, which makes it possible to discriminate between beam-beam and beam-gas events, in which beam particles interact with residual gas inside the beam pipe. The raw signals of the V0 and AD detectors are used in the trigger. Off-line, these detectors are used to differentiate beam-beam and beam-gas interactions.

The two ZDCs are located at 112.5 m from the nominal interaction point along the beam axis on either side of the ALICE detector. They are used to detect neutrons emitted in the very forward region and measure timing information of signals, thus making possible the discrimination of background signals such as beam-satellite events described in Ref. [51].

Exclusive dimuon production from the decay of a J/ψ or from two-photon interactions has a clear experimental signature: the $\mu^+\mu^-$ pair in an otherwise empty detector. On the other hand, the study of J/ψ photoproduction with a dissociative proton implies that the detector might not be empty on the proton side. The trigger used in these analyses

[1]In the ALICE convention, the muon spectrometer lies at negative longitudinal coordinate z, where $z = 0$ is the nominal interaction point position, therefore at negative pseudorapidity.

is required to have at least one track with a low transverse momentum threshold ($p_T \sim 0.5$ GeV/c) in the muon spectrometer trigger system and vetoes on V0A and ADA which are located in the flight direction of the outgoing Pb ion.

The measurements presented here use a sample of events collected during the 2016 p-Pb data taking period, at $\sqrt{s_{NN}} = 8.16$ TeV, corresponding to an integrated luminosity of $\mathcal{L} = 7.90 \pm 0.14$ nb^{-1} [52]. In these collisions the incoming proton beam traveled toward the muon spectrometer.

III. DATA SAMPLE

A. Event selection

Besides the trigger selection, events have to fulfill additional criteria. First, there must be exactly two tracks with opposite electric charge reconstructed in the muon spectrometer. Both tracks are required to match muon trigger tracks with a p_T threshold above 0.5 GeV/c. Each track pseudorapidity is required to be within the acceptance of the muon spectrometer $-4.0 < \eta < -2.5$. To reject tracks crossing the high-density section of the front absorber, where multiple scattering and energy loss effects are large, the muon tracks are required to exit the front absorber at a radial distance from the beam axis $17.6 < R_{abs} < 89.5$ cm. The product of the total track momentum p and the distance of closest approach, defined as the distance in the transverse plane between the extrapolated position of the reconstructed track in the tracking stations and the position of the nominal interaction point, is required to be smaller than 6 times the standard deviation of the dispersion due to multiple scattering and detector resolution. This ensures that the selected muons come from the interaction vertex without rejecting signal events. The dimuon rapidity has to be in the range $2.5 < y < 4.0$, and the dimuon p_T must be less than 3 GeV/c.

To ensure that the Pb ion remains intact, the V0A and ADA are required to have no signal at the off-line level. The neutron ZDC on the Pb side (ZNA) must have no activity within ± 2 ns of the expected time of the collision. In order to suppress hadronic interactions producing particles at midrapidity, events with more than two tracklets in the SPD layers are rejected.

Finally, the number of cells with a signal over threshold in V0C must be smaller than or equal to the sum of the number of fired V0C cells matched to a muon and two additional fired cells. The matching of a muon to a fired V0C cell is performed by using the (η, φ) coordinates of each track, where φ is the azimuthal coordinate. Studies with the RAPGAP 3.3 event generator [53], a Monte Carlo program used to simulate dissociative J/ψ photoproduction in electron-proton collisions, show that the proton remnants do not leave a signal in the acceptance of the V0C detector. The requirement on the number of fired V0C cells prevents contamination from hadronic interactions at forward rapidity.

Allowing two midrapidity tracklets in the SPD layers and two additional fired V0C cells prevents detectors from vetoing events of interest due to an additional activity, such as muon bremsstrahlung or pileup events. Pileup events are induced mainly by independent hadronic or electromagnetic processes, e.g. dielectron production in the $\gamma\gamma \to e^+e^-$ process, accompanying the process of interest.

B. Event selection with exclusivity in the proton side

The exclusive-dominated sample is obtained by applying the following additional criteria on the proton side. The ADC is required to have no signal and the neutron ZDC on the proton side must have no activity within ± 6 ns of the expected time of the collision. This selection is more restrictive than on the Pb side, due to an observed asymmetry of time distributions between both sides. Furthermore, since exclusive events are expected to be dominant at low p_T, dimuons are required to have $p_T < 1.2$ GeV/c.

IV. MONTE CARLO SAMPLES

The STARlight 2.2.0 Monte Carlo generator [22,54] is used to generate the following processes: exclusive J/ψ production in γp interactions, production of J/ψ in γPb interactions, production of J/ψ events from decays of $\psi(2S)$ in γp interactions, and exclusive dimuon continuum production. The decay muons are propagated through a model of the apparatus implemented in GEANT 3.21 [55], and events pass through a simulation of the detector matching the data taking conditions. For exclusive J/ψ production, the t distribution is modeled in STARlight by a function of the form $\exp(-bt)$, where b is set to 3.75 GeV^{-2} to better describe the J/ψ p_T distribution in data.

V. DATA ANALYSIS

A. Signal extraction for the two-photon process at low masses

The yields of dimuons from exclusive two-photon interactions, $N_{\gamma\gamma}$, are measured by performing an unbinned log-likelihood fit of the p_T distribution up to $p_T = 3$ GeV/c of the selected dimuons in the invariant mass range $1.0 < M_{\mu\mu} < 2.5$ GeV/c^2, where no contamination is expected from the J/ψ peak. The measurements are performed as a function of the dimuon invariant mass, in the three intervals $1.0 < M_{\mu\mu} < 1.5$, $1.5 < M_{\mu\mu} < 2.0$, and $2.0 < M_{\mu\mu} < 2.5$ GeV/c^2. They are presented in the rapidity interval $2.5 < y < 4.0$, and for $2.5 < y < 3.25$ and $3.25 < y < 4.0$, where the rapidity is measured in the laboratory frame with respect to the proton beam direction.

Figure 1 shows the p_T distribution of the dimuon candidates that satisfy the selections for $1.5 < M_{\mu\mu} < 2.0$ GeV/c^2. The data contain a mixture of exclusive and nonexclusive two-photon interactions, which are distinguished by their characteristic p_T distribution. While

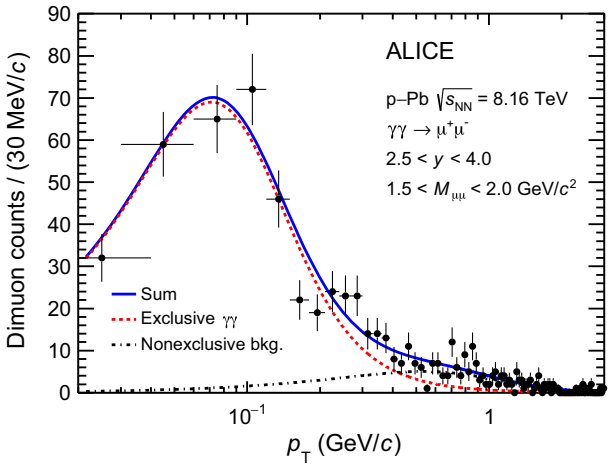

FIG. 1. Transverse momentum distribution of opposite-sign dimuons with $1.5 < M_{\mu\mu} < 2.0$ GeV/c^2 and $2.5 < y < 4.0$. The data are represented by full circles with vertical bars for the statistical uncertainties and horizontal bars for the interval width. The solid line represents the fit to the data, and the dashed and dot-dashed lines represent the fit components.

exclusive events dominate in the data at low p_T, the tail extending up to higher p_T is mostly due to nonexclusive interactions.

Exclusive $\gamma\gamma \to \mu^+\mu^-$ events are described with a Landau distribution, which is found to describe well the Monte Carlo data up to $p_T = 0.38$ GeV/c. A single-component fit of a Landau distribution is performed to the data requiring exclusivity on the proton side, as described in Sec. III B, up to $p_T = 0.38$ GeV/c. In this selection, nonexclusive events are expected to be negligible. The location and scale parameters of the Landau distribution are extracted. The obtained location parameter ranges between 0.054 and 0.092 for the different bins. The scale parameter ranges between 0.23 and 0.39. They are then used when fitting the data that passed the standard selection, which includes both exclusive and nonexclusive components. Changing the maximum p_T value of the fitting interval or using a two-component model to account for exclusive and nonexclusive events instead of a single-component description might impact the location and scale parameters obtained from the fit of the exclusive-dominated sample. This is taken into account in the "signal extraction" systematic uncertainty (see Sec. V C 2).

Nonexclusive events are modeled according to a parametrization by H1 for dissociative events [40] with a function of the form $\mathrm{d}N/\mathrm{d}p_T \propto p_T \times (1 + p_T^2 \times (b_{\mathrm{dis}}/n_{\mathrm{dis}}))^{-n_{\mathrm{dis}}}$, where b_{dis} and n_{dis} are free parameters. Nonexclusive dimuons represent 37% of events in the analyzed mass range and for $p_T < 3$ GeV/c.

The $N_{\gamma\gamma}$ yields extracted from the fit are then corrected for the acceptance and reconstruction efficiency $(A \times \epsilon)^{\gamma\gamma}$. The yields, the correction factors, and the cross sections are presented in Table II for the different mass and rapidity intervals. The correction factors are evaluated by means of the Monte Carlo simulations introduced in Sec. IV.

Additional activity in the V0A, ADA, ZNA, or SPD detectors results in event rejection and a corresponding correction needs to be applied. Such events mainly originate from independent hadronic and electromagnetic pileup processes. The probability of event rejection due to pileup of each veto is defined as the probability of detecting activity using events selected with an unbiased trigger based only on the timing of bunches crossing the interaction region. It is found to scale linearly with the expected number of collisions per bunch crossing. By varying the event selection in the analysis, the average pileup probability varied from 3.7% to 4.1%. Therefore, the pileup probability is estimated as $p_{\mathrm{pu}} = (3.9 \pm 0.2)\%$ where most of the pileup rejection (3.7%) is from V0A. The average pileup correction factor is calculated using $\epsilon_{\mathrm{veto}} = \exp(-p_{\mathrm{pu}})$ and is found to be $\epsilon_{\mathrm{veto}} = (96.2 \pm 0.2)\%$.

B. Signal extraction for J/ψ photoproduction candidates

The yields of exclusive and dissociative J/ψ are obtained by performing an unbinned log-likelihood fit to dimuon invariant mass $M_{\mu\mu}$ and transverse momentum p_T distributions simultaneously. Events are selected in $2.5 < M_{\mu\mu} < 3.5$ GeV/c^2 and $p_T < 3$ GeV/c intervals. The dimuon invariant mass and p_T spectra after these selections are shown in Fig. 2. For the invariant mass distribution, the J/ψ peak is well described by a double-sided Crystal Ball parametrization, which has a non-Gaussian tail at both sides of the resonance peak [56,57]. The J/ψ mass and its width at the pole position are free parameters of the fit, while the tail parameters in the Crystal Ball function are fixed to values obtained from fits to the Monte Carlo sample corresponding to the exclusive J/ψ photoproduction. The invariant mass distribution of the dimuon continuum is described by $\mathrm{d}N/\mathrm{d}M_{\mu\mu} \propto \exp(-aM_{\mu\mu})$, where a is a free parameter.

J/ψ events can be divided into three categories: exclusive photoproduction off protons, dissociative photoproduction off protons, and exclusive photoproduction off Pb nuclei. Dissociative photoproduction off Pb nuclei is vetoed by the ZDC selection, as described in Sec. III A. The events contained in the dimuon continuum below the J/ψ peak can either be exclusive or nonexclusive two-photon interactions. The various physics processes in the J/ψ peak and in the dimuon continuum can be distinguished by their different p_T distributions.

The p_T distribution for $\gamma\gamma \to \mu^+\mu^-$ events below the J/ψ peak is modeled with a Landau distribution for which the location and scale parameters are fixed, similarly as in Sec. V A. Their values are obtained using the sample described in Sec. III B. In order to factorize the p_T distribution of J/ψ and continuum dimuon events, the

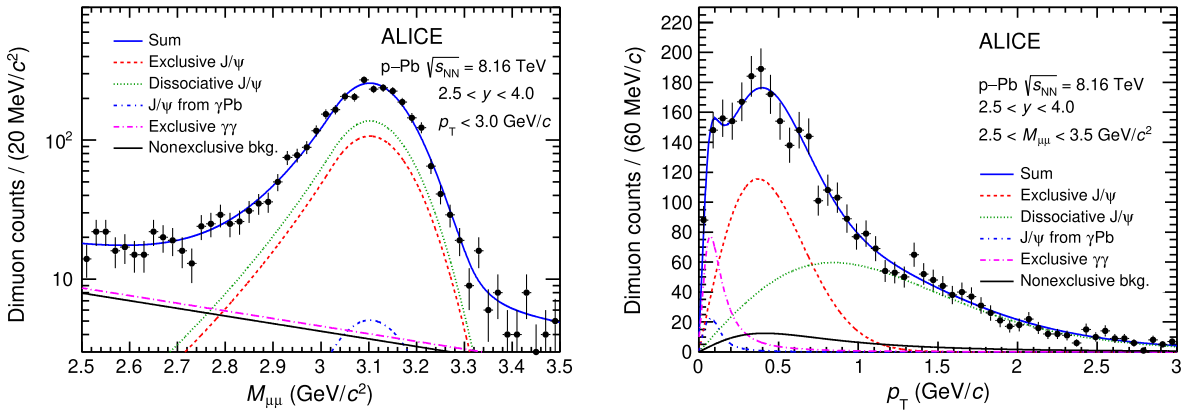

FIG. 2. Projections of the two-dimensional fit on the dimuon invariant mass (left) and p_T (right).

numerical tool sPlot is used [58]. Based on an extended maximum likelihood fit to the mass distribution of the sample (left panel of Fig. 3), the sPlot procedure assigns weights denoted as sw_n on an event-by-event basis. Assuming these weights can be computed as a linear combination of conditional probabilities, they are given by the following formula for the category $n = 1, 2$ of events in the sample (J/ψ signal or $\gamma\gamma \to \mu^+\mu^-$)

$$sw_n(M_{\mu\mu}) = \frac{\sum_{i=1}^{N_s} V_{ni} f_i(M_{\mu\mu})}{\sum_{j=1}^{N_s} N_j f_j(M_{\mu\mu})}, \tag{1}$$

where f is the probability density function of the fit, $M_{\mu\mu}$ denotes the mass used as the discriminating variable for each event, i and j are the indices indicating a sum over the $N_s = 2$ categories, and V is the covariance matrix of the yields N_j which is evaluated in a separate fit, in which all shape-related parameters are fixed. The p_T distribution for two-photon interactions extracted with the sPlot technique is shown in the right panel of Fig. 3 and is fitted up to $p_T = 0.38$ GeV/c with a single-component fit parametrized with a Landau distribution, from which the location and scale parameters are extracted. The small correlation between the mass and p_T of dimuons produced in two-photon interactions was found to have a negligible impact on the sPlot procedure. In addition, the extracted number of $\gamma\gamma \to \mu^+\mu^-$ events in the J/ψ peak range ($2.5 < M_{\mu\mu} < 3.5$ GeV/c^2) is compared with STARlight and an agreement within 1σ is found (accounting for the statistical uncertainties only). This number is also in good agreement with the number of continuum dimuon events extracted from the final two-dimensional fit.

The shape of the p_T distribution for the exclusive J/ψ events in γp interactions is given by the H1 parametrization [40] $dN/dp_T \propto p_T \times \exp(-b_{exc} p_T^2)$, where b_{exc} is a fixed parameter. J/ψ mesons coming from $\psi(2S)$ decays are also included in this contribution. The b_{exc} value is determined using the sample described in Sec. III B, by fitting simultaneously the dimuon invariant mass and p_T without the contribution of dissociative J/ψ events. The dimuon invariant mass and p_T projections of this fit are shown in Fig. 4.

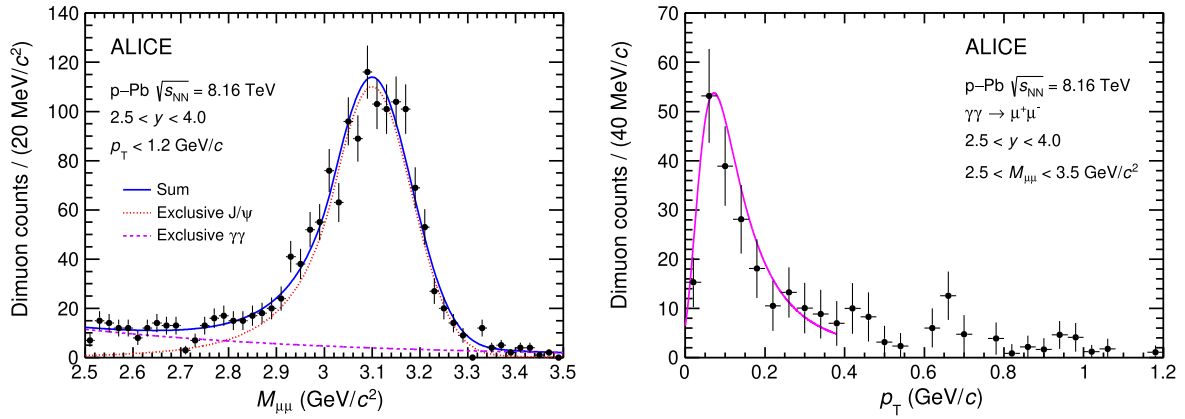

FIG. 3. Left: dimuon invariant mass distribution using the selection given in Sec. III B, fitted with a two-component model to separate J/ψ events from two-photon interactions in the continuum. Right: p_T distribution of the exclusive $\gamma\gamma \to \mu^+\mu^-$ continuum extracted using the sPlot technique. The distribution is fitted with a Landau distribution.

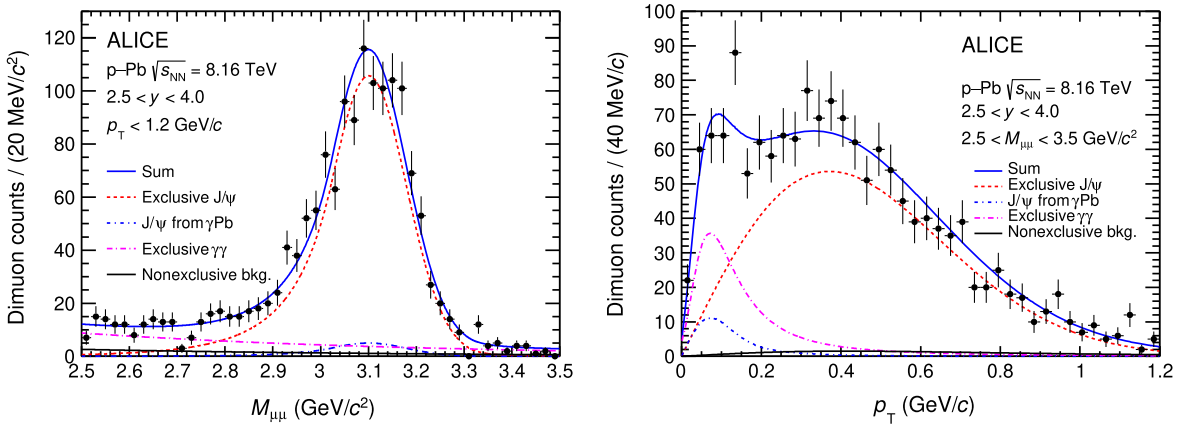

FIG. 4. Projections of the two-dimensional fit on the dimuon invariant mass (left) and p_T (right) with the selection described in Sec. III B to extract the shape of the p_T distribution for the exclusive J/ψ events in γp interactions.

Studies conducted with the RAPGAP Monte Carlo program [53] in the kinematic range of the present measurement show that more than 99% of dissociative J/ψ events are removed by the selection requiring exclusivity on the proton side. The values obtained are $b_{\rm exc} = 3.62 \pm 0.14$ $[\mathrm{GeV}/c]^{-2}$ for $2.5 < y_{\mu\mu} < 4.0$, $b_{\rm exc} = 3.38 \pm 0.17$ $[\mathrm{GeV}/c]^{-2}$ for $3.25 < y_{\mu\mu} < 4.0$ $(27 < W_{\gamma\mathrm{p}} < 39$ GeV), and $b_{\rm exc} = 3.86 \pm 0.20$ $[\mathrm{GeV}/c]^{-2}$ for $2.5 < y_{\mu\mu} < 3.25$ $(39 < W_{\gamma\mathrm{p}} < 57$ GeV). The p_T resolution of the muon spectrometer is the main limitation in unfolding these values and comparing them with the H1 measurement of the t slope, $b_{\rm exc} = (4.3 \pm 0.2)$ $[\mathrm{GeV}]^{-2}$ for $25 < W_{\gamma\mathrm{p}} < 80$ GeV [40]. As an alternative method to extract the $b_{\rm exc}$ value, the J/ψ p_T distribution obtained with sPlot was fitted with a two-component model including J/ψ events from γp interactions and from γPb interactions. The bias induced by the method used to extract $b_{\rm exc}$ is accounted for in the signal extraction systematic uncertainty (see Sec. V C 3).

The p_T distribution for coherent J/ψ photoproduction in γPb interactions is obtained using the corresponding reconstructed Monte Carlo sample within the specified mass and p_T ranges. The p_T distributions for dissociative J/ψ events and nonexclusive two-photon interactions are modeled by functions of the form $\mathrm{d}N/\mathrm{d}p_T \propto p_T \times (1 + p_T^2 \times (b_{\rm dis}/n_{\rm dis}))^{-n_{\rm dis}}$ where $b_{\rm dis}$ and $n_{\rm dis}$ are free parameters.

Five parametrizations for exclusive J/ψ photoproduction off protons, dissociative J/ψ photoproduction off protons, J/ψ photoproduction off Pb nuclei, exclusive, and nonexclusive $\gamma\gamma \to \mu^+\mu^-$, are defined as products of each corresponding mass and p_T distributions. The normalization for the component corresponding to J/ψ produced in γPb interactions is fixed to the expected number according to a computation based on the measurement from Ref. [59] under the assumption that the fraction of low- and high-energy photon contributions to the forward rapidity measurement is the same as predicted by STARlight. The normalization for all other components are free parameters of the fit.

The extracted yields of exclusive and dissociative J/ψ from γp interactions are corrected for acceptance and reconstruction efficiency $(A \times \epsilon)^{J/\psi}$, which are obtained from the Monte Carlo simulation samples described in Sec. IV, having values ranging from 18% to 21%.

The extracted yields are corrected for the feed-down contribution of J/ψ mesons coming from $\psi(2S)$ decays, denoted $f_{\rm D}$. Following the procedure described in Ref. [13], $f_{\rm D}$ is given by

$$f_{\rm D} = \frac{\sigma(\psi(2S)) \times \mathrm{BR}(\psi(2S) \to J/\psi + X) \times (A \times \epsilon)^{\rm FD}_{J/\psi}}{\sigma(J/\psi) \times (A \times \epsilon)_{J/\psi}}, \quad (2)$$

where $\sigma(J/\psi)$ and $\sigma(\psi(2S))$ are the cross sections of J/ψ and $\psi(2S)$ productions, respectively, at a given rapidity, the branching ratio for the decay of a $\psi(2S)$ to J/ψ is $\mathrm{BR}(\psi(2S) \to J/\psi + X) = (61.4 \pm 0.6)\%$ [60], and $(A \times \epsilon)_{J/\psi}$ and $(A \times \epsilon)^{\rm FD}_{J/\psi}$ are the acceptance and reconstruction efficiency for events with a J/ψ produced directly from γp interactions and from $\psi(2S)$ decays, respectively. In order to compute $f_{\rm D}$, the ratio $\sigma(\psi(2S))/\sigma(J/\psi) = 0.150 \pm 0.013(\mathrm{stat}) \pm 0.011(\mathrm{syst})$ is taken from the H1 measurement for $40 < W_{\gamma\mathrm{p}} < 70$ GeV [61]. The $(A \times \epsilon)^{\rm FD}_{J/\psi}$ values are evaluated under the assumption that feed-down J/ψ mesons inherit the transverse polarization of their $\psi(2S)$ parents, as indicated by previous measurements [62]. The obtained $f_{\rm D}$ values range between $(9.1 \pm 1.2)\%$ and $(9.3 \pm 1.2)\%$ depending on the rapidity interval. The uncertainties are obtained by summing the statistical and systematic uncertainties of the H1 measurement and branching ratio uncertainties in quadrature. Finally, the numbers are corrected for pileup, as discussed in Sec. V A.

C. Systematic uncertainties

The experimental systematic uncertainties for the exclusive dimuon production from two-photon interactions and for the photoproduced J/ψ are listed in Table I. The systematic sources can be divided into three types: those common to both measurements and those affecting one or the other.

1. Systematic uncertainties common to both measurements

The uncertainty on the integrated luminosity is discussed in Sec. II and amounts to 1.8%. The systematic uncertainties on muon trigger efficiency, tracking efficiency, and muon matching efficiency were obtained as described in Ref. [63]. The single-muon trigger response functions evaluated in data and Monte Carlo simulations are incorporated in the acceptance and efficiency $(A \times \epsilon)$ calculations for the reconstruction of the dimuons. The differences between $(A \times \epsilon)$ calculations when incorporating the response functions either from data or Monte Carlo range from 0.1% to 4.9% depending on the studied process and rapidity interval. The total uncertainty is obtained by combining this contribution in quadrature with the uncertainty on the intrinsic efficiency of muon trigger detectors, which amounts to 1%.

The uncertainty on the tracking efficiency was calculated by comparing the efficiencies evaluated in data and Monte Carlo simulations. These efficiencies are calculated according to the tracking algorithm by combining the efficiency of each tracking plane measured using the redundancy of the system. The estimated value of the systematic

TABLE I. Summary of systematic uncertainties on the measured cross sections. The value ranges correspond to different rapidity intervals. Uncertainties on signal extraction, tracking, trigger, and muon matching efficiencies are considered as uncorrelated across y. All other components are taken as fully correlated across the rapidity y. The final uncertainties for $\gamma\gamma$ and J/ψ, labeled "Total," are obtained as the sum in quadrature of common uncertainties and those affecting one signal or the other.

Signal	Source	Mass range (GeV/c^2)	Value (%)
All	Luminosity		1.8
	Tracking efficiency		1
	Matching efficiency		1
	Pileup correction		0.2
	Total common		2.3
$\gamma\gamma$ only	Muon trigger efficiency	(1.0, 1.5)	From 2.1 to 3.4
		(1.5, 2.0)	From 2.5 to 5.0
		(2.0, 2.5)	From 1.6 to 3.3
	$\phi \to \mu^+\mu^-$ contamination	(1.0, 1.5)	1.5
	V0C veto	(1.0, 1.5)	1.2
		(1.5, 2.0)	1.7
		(2.0, 2.5)	0.5
	Signal extraction	(1.0, 1.5)	From 3.2 to 3.9
		(1.5, 2.0)	From 3.3 to 4.4
		(2.0, 2.5)	From 4.9 to 7.6
	Total	(1.0, 1.5)	From 4.9 to 6.0
		(1.5, 2.0)	From 5.5 to 7.1
		(2.0, 2.5)	From 6.0 to 8.6
J/ψ only	Muon trigger efficiency		1.1
	Branching ratio		0.55
	Photon flux		2
	$\delta(1 + f_D)$		1.1
	V0C veto		2.6 (excl.), 12.7 (diss.)
	Signal extraction	(2.5, 3.5)	From 3.6 to 5.5 (excl.) From 2.9 to 4.4 (diss.)
	Total		From 5.6 to 7.0 (excl.) From 13.5 to 13.9 (diss.)
$\frac{\sigma^{\text{diss}}}{\sigma^{\text{exc}}}$	V0C veto		12.7
	Signal extraction		From 6.2 to 7.6
	Total		From 14.1 to 14.8

uncertainty related to the tracking efficiency is 1% in this data sample. The muon matching efficiency is the efficiency of associating a muon track candidate to a trigger track above the 0.5 GeV/c p_{T} threshold in the trigger chambers of the muon spectrometer. Its uncertainty is estimated by varying the χ^2 cutoff applied to the pairing of the reconstructed tracks in the muon tracking and triggering systems, and it is found to be 1%.

The pileup correction factor, discussed in Sec. V A, has a relative uncertainty of 0.2%.

The uncertainty on the veto efficiency of the V0C is calculated by varying the number of allowed cells with a signal over the threshold in the off-line selection. When increasing this number, the numbers of exclusive J/ψ and $\gamma\gamma \to \mu^+\mu^-$ events are found to be stable, while the number of dissociative J/ψ events increases, as the sample is more sensitive to contamination from inclusive photoproduction or hadronic production of J/ψ mesons which have a similar behavior in p_{T}. The expected number of dissociative J/ψ events is computed as the number of exclusive J/ψ events multiplied by the ratio of dissociative-to-exclusive J/ψ events when all the fired cells in V0C are required to be matched to a muon. The systematic uncertainty on the number of dissociative J/ψ events is computed as the relative difference between the expected and extracted numbers of dissociative J/ψ events and is found to be 12.7%, while the systematic uncertainty on the number of exclusive J/ψ events is obtained by varying the condition on V0C and the obtained value is 2.6%. Similarly, the uncertainty on the number of exclusive $\gamma\gamma \to \mu^+\mu^-$ events is obtained by varying the condition on V0C (see line "V0C veto" in Table I) and the obtained values vary between 0.5% and 1.7%.

2. Uncertainties associated with the dimuon continuum production

The main source of systematic uncertainty on the $\gamma\gamma \to \mu^+\mu^-$ signal extraction is obtained by varying both parameters of the Landau distribution within their statistical uncertainties obtained from fitting the purely exclusive sample described in Sec. III B and taking into account their correlation (see line signal extraction in Table I).

In the lowest invariant mass interval studied, $1.0 < M_{\mu\mu} < 1.5$ GeV/c^2, the production of ϕ mesons decaying to dimuons might contaminate the sample. The expected number of $\phi \to \mu^+\mu^-$ events in the sample at low mass, N_ϕ, is computed. The calculation is based on the cross section ratio of ϕ photoproduction with respect to J/ψ production based on STARlight and their branching ratios provided by the PDG [60], detector acceptance and efficiency factors, and the number of J/ψ mesons measured in the muon spectrometer. The uncertainty induced by this contamination is estimated by comparing N_ϕ to the number of $\gamma\gamma \to \mu^+\mu^-$ events. It is found to be 1.5%.

3. Uncertainties associated with the J/ψ photoproduction only

The main source of systematic uncertainty on the J/ψ signal extraction is obtained by varying the b_{exc} parameter within its statistical uncertainty determined from fitting the purely exclusive sample described in Sec. III B (see line signal extraction in Table I). It ranges between 2.9% and 5.5%. Changing the p_{T} model for the exclusive $\gamma\gamma \to \mu^+\mu^-$ component and varying the number of J/ψ events produced in γPb interactions was found to have a negligible impact on signal extraction.

The photon flux, which enters in the computation of the cross section presented in Sec. VI B, is computed using STARlight. Its uncertainty is obtained by varying the nuclear radii and the nuclear density ρ_0 of the Pb nucleus, assuming that the latter has a cubic dependence on the radius. The radius of the lead nucleus is changed by ± 0.5 fm, which corresponds to the nuclear skin thickness. This uncertainty is evaluated to be 2%. The branching ratio of J/ψ decaying into dimuons and its uncertainty (0.55%) are given by the Particle Data Group [60].

For the measured ratio of dissociative-to-exclusive cross sections, $\sigma^{\mathrm{diss}}/\sigma^{\mathrm{exc}}$, most of the systematic uncertainties cancel out. The remaining sources of uncertainty are due to the variation of the b_{exc} parameter and the variation on the number of allowed fired V0C cells. The systematic uncertainties on the ratio given in Table I are then computed as the quadratic sum of these two components only.

VI. RESULTS

A. Cross sections for the dimuon continuum in two-photon interactions

The cross section corresponding to the exclusive $\gamma\gamma \to \mu^+\mu^-$ process is measured using

$$\frac{\mathrm{d}\sigma^{\gamma\gamma}}{\mathrm{d}M_{\mu\mu}}(\mathrm{p} + \mathrm{Pb} \to \mathrm{p} + \mathrm{Pb} + \mu^+ + \mu^-) = \frac{N_{\gamma\gamma}}{(A \times \epsilon)^{\gamma\gamma} \times \mathcal{L} \times \epsilon_{\mathrm{veto}} \times \Delta M_{\mu\mu}}, \tag{3}$$

where $N_{\gamma\gamma}$ is the number of reconstructed $\gamma\gamma \to \mu^+\mu^-$ events, $(A \times \epsilon)^{\gamma\gamma}$ is the corresponding factor which takes into account acceptance and reconstruction efficiency in the mass and rapidity interval studied, ϵ_{veto} is the pileup correction factor, and $\Delta M_{\mu\mu}$ is the width of the invariant mass interval.

The rapidity range of the experimental results corresponds to a high-energy photon emitted from the proton (corresponding to small impact parameters with respect to the proton) and a low-energy photon emitted from the nucleus (corresponding to large impact parameters with respect to the nucleus). The differential cross sections, $\mathrm{d}\sigma^{\gamma\gamma}/\mathrm{d}M_{\mu\mu}$, are presented in Table II in two rapidity intervals and integrated over rapidity along with the

TABLE II. Differential cross sections $\mathrm{d}\sigma^{\gamma\gamma}/\mathrm{d}M_{\mu\mu}$ for exclusive $\gamma\gamma \to \mu^+\mu^-$ production in p-Pb UPCs at $\sqrt{s_{\mathrm{NN}}} = 8.16$ TeV for each mass and rapidity interval, measured by ALICE and computed with STARlight and SuperChic. The first uncertainty is the statistical one and the second uncertainty is the systematic one. The corresponding number of exclusive $\gamma\gamma \to \mu^+\mu^-$ events with their statistical uncertainties and factors of acceptance times reconstruction efficiency are given.

Mass range (GeV/c^2)	Rapidity range	$N_{\gamma\gamma}$	$(A \times \epsilon)$ (%)	$\mathrm{d}\sigma^{\gamma\gamma}/\mathrm{d}M_{\mu\mu}$ (μb c^2/GeV)	$\mathrm{d}\sigma^{\gamma\gamma}/\mathrm{d}M_{\mu\mu}$ (μb c^2/GeV) (STARlight)	$\mathrm{d}\sigma^{\gamma\gamma}/\mathrm{d}M_{\mu\mu}$ (μb c^2/GeV) (SuperChic)
(1.0, 1.5)	(2.5, 4)	618 ± 33	1.66	$9.84 \pm 0.52 \pm 0.49$	8.45	8.98
	(3.25, 4)	522 ± 31	3.23	$4.26 \pm 0.25 \pm 0.20$	4.05	4.33
	(2.5, 3.25)	99 ± 11	0.45	$5.75 \pm 0.67 \pm 0.34$	4.39	4.65
(1.5, 2.0)	(2.5, 4)	437 ± 26	3.04	$3.79 \pm 0.22 \pm 0.20$	3.00	3.22
	(3.25, 4)	283 ± 19	4.74	$1.58 \pm 0.12 \pm 0.09$	1.44	1.55
	(2.5, 3.25)	150 ± 14	1.82	$2.17 \pm 0.20 \pm 0.15$	1.56	1.67
(2.0, 2.5)	(2.5, 4)	191 ± 18	4.09	$1.23 \pm 0.12 \pm 0.07$	1.42	1.52
	(3.25, 4)	103 ± 13	5.32	$0.511 \pm 0.065 \pm 0.034$	0.673	0.724
	(2.5, 3.25)	85 ± 13	3.25	$0.692 \pm 0.101 \pm 0.060$	0.744	0.794

predictions from STARlight 2.2.0 and SuperChic 4.15 [64] for comparison.

The STARlight generator simulates UPCs at colliders based on the equivalent photon approximation. SuperChic was designed for exclusive production in proton-proton collisions and has been extended to collisions involving nuclei starting from Ref. [65]. For $\gamma\gamma$-induced dilepton production, SuperChic provides calculations on amplitude level to treat the probability of no hadronic interaction within the same collision. Both generators implement LO QED calculations, neglecting final-state radiation.

The measured cross sections and predictions from STARlight and SuperChic are shown in Fig. 5. Both predictions agree within 3 standard deviations, depending on the mass and rapidity intervals. In the two lowest mass intervals, the central values of the measured cross sections are larger compared with STARlight and SuperChic, while the opposite behavior is seen in the highest mass interval. For the kinematic intervals studied, SuperChic predicts larger cross sections than STARlight. The difference between STARlight and SuperChic discussed in Ref. [23], related to the sharp cutoff on the impact parameter between the produced dilepton and the nucleus, is found not to be the primary source of discrepancy observed here.

The relative uncertainties on the measurements vary from 7% to 17%. This is significantly larger than the 2% uncertainty for the photon flux used in the calculation of the photoproduction cross section presented in Sec. VI B. Thus, with the current experimental precision, it is not possible to constrain the photon fluxes via the $\gamma\gamma \to \mu^+\mu^-$ measurement.

B. Cross sections for J/ψ photoproduction off protons

The cross sections corresponding to exclusive and dissociative J/ψ photoproduction off protons are measured using

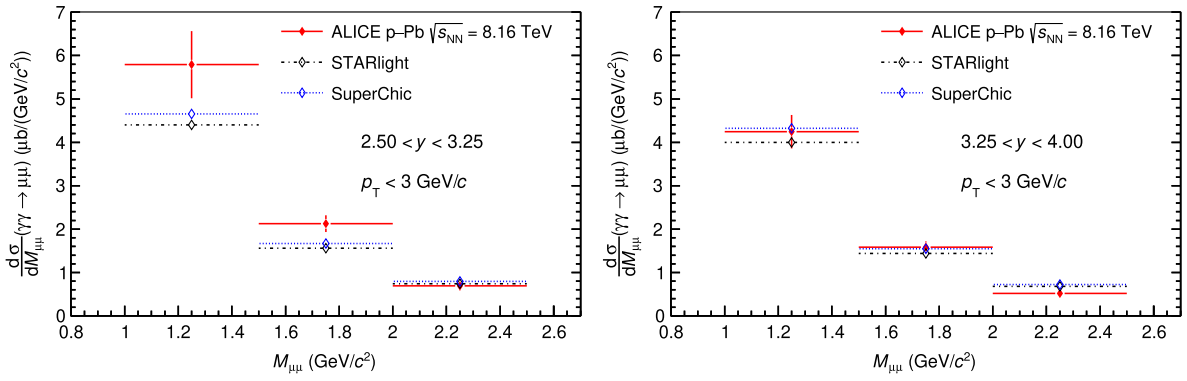

FIG. 5. Differential cross sections for exclusive $\gamma\gamma \to \mu^+\mu^-$ production measured by ALICE in p-Pb UPCs at $\sqrt{s_{\mathrm{NN}}} = 8.16$ TeV, as a function of $M_{\mu\mu}$, for $2.5 < y < 3.25$ (left) and $3.25 < y < 4$ (right). The vertical error bars represent the statistical and systematic uncertainties summed in quadrature. The results are compared with the prediction from STARlight [22,54] and from SuperChic [64].

TABLE III. Rapidity differential cross sections $\mathrm{d}\sigma^{\mathrm{exc}}_{J/\psi}/\mathrm{d}y$ and $\mathrm{d}\sigma^{\mathrm{diss}}_{J/\psi}/\mathrm{d}y$ and the corresponding cross sections $\sigma(\gamma + \mathrm{p} \to J/\psi + \mathrm{p})$ and $\sigma(\gamma + \mathrm{p} \to J/\psi + \mathrm{p}^{(*)})$ for exclusive and dissociative J/ψ photoproduction off protons in p-Pb UPCs at $\sqrt{s_{\mathrm{NN}}} = 8.16$ TeV for each rapidity range. The first uncertainty is the statistical one and the second uncertainty is the systematic one. The numbers of events obtained from signal extraction with their statistical uncertainties, $N^{\mathrm{exc}}_{J/\psi}$ and $N^{\mathrm{diss}}_{J/\psi}$, the photon flux, and the range and the mean of $W_{\gamma\mathrm{p}}$ are also presented.

Rapidity range	$N^{\mathrm{exc}}_{J/\psi}$, $N^{\mathrm{diss}}_{J/\psi}$	$\mathrm{d}\sigma^{\mathrm{exc}}_{J/\psi}/\mathrm{d}y$, $\mathrm{d}\sigma^{\mathrm{diss}}_{J/\psi}/\mathrm{d}y$ (μb)	$k\mathrm{d}n/\mathrm{d}k$	$W_{\gamma\mathrm{p}}$ (GeV)	$\langle W_{\gamma\mathrm{p}} \rangle$ (GeV)	$\sigma(\gamma + \mathrm{p} \to J/\psi + \mathrm{p})$ (nb), $\sigma(\gamma + \mathrm{p} \to J/\psi + \mathrm{p}^{(*)})$ (nb)
(2.5, 4)	1180 ± 84 1515 ± 83	$8.13 \pm 0.58 \pm 0.43$ $10.43 \pm 0.57 \pm 1.39$	209 ± 4	(27, 57)	39.9	$39.0 \pm 2.8 \pm 2.2$ $50.0 \pm 2.7 \pm 6.7$
(3.25, 4)	564 ± 53 733 ± 52	$7.16 \pm 0.67 \pm 0.48$ $9.31 \pm 0.66 \pm 1.28$	220 ± 4	(27, 39)	32.8	$32.51 \pm 3.0 \pm 2.3$ $42.3 \pm 3.0 \pm 5.9$
(2.5, 3.25)	629 ± 54 768 ± 55	$9.21 \pm 0.80 \pm 0.51$ $11.26 \pm 0.80 \pm 1.53$	197 ± 4	(39, 57)	47.7	$46.8 \pm 4.1 \pm 2.8$ $57.2 \pm 4.1 \pm 7.8$

$$\frac{\mathrm{d}\sigma}{\mathrm{d}y}(\mathrm{p} + \mathrm{Pb} \to p^{(*)} + \mathrm{Pb} + J/\psi) = \frac{N_{J/\psi}}{(A \times \epsilon)^{J/\psi} \times (1 + f_{\mathrm{D}}) \times \mathcal{L} \times \epsilon_{\mathrm{veto}} \times \mathrm{BR} \times \Delta y}, \quad (4)$$

where $N_{J/\psi}$ is the number of reconstructed exclusive or dissociative J/ψ in the dimuon decay channel, $(A \times \epsilon)^{J/\psi}$ is the corresponding factor of acceptance times reconstruction efficiency in the rapidity interval studied, and $\mathrm{BR} = (5.961 \pm 0.033)\%$ is the branching ratio for the decay into a muon pair [60].

The cross section $\mathrm{d}\sigma/\mathrm{d}y(\mathrm{p} + \mathrm{Pb} \to p^{(*)} + \mathrm{Pb} + J/\psi)$ is related to the $\gamma\mathrm{p}$ cross section $\sigma(\gamma + \mathrm{p} \to J/\psi + p^{(*)})$ through the photon flux $\mathrm{d}n/\mathrm{d}k$,

$$\frac{\mathrm{d}\sigma}{\mathrm{d}y}(\mathrm{p} + \mathrm{Pb} \to p^{(*)} + \mathrm{Pb} + J/\psi) = k\frac{\mathrm{d}n}{\mathrm{d}k}\sigma(\gamma + \mathrm{p} \to J/\psi + p^{(*)}). \quad (5)$$

Here, k is the photon energy, which is determined by the J/ψ mass and rapidity, $k = (1/2)M_{J/\psi}\exp(-y)$. The photon flux is calculated using STARlight in impact parameter space and convoluted with the probability of no hadronic interaction. The average photon flux values for the different rapidity intervals are listed in Table III, together with the extracted cross sections $\sigma(\gamma + \mathrm{p} \to J/\psi + \mathrm{p})$ and $\sigma(\gamma + \mathrm{p} \to J/\psi + \mathrm{p}^{(*)})$ and the corresponding $\langle W_{\gamma\mathrm{p}} \rangle$. The latter is computed as the average of $W_{\gamma\mathrm{p}}$ weighted by the cross section $\sigma(\gamma\mathrm{p})$ from STARlight.

1. Exclusive J/ψ photoproduction

Figure 6 shows the exclusive J/ψ photoproduction cross section $\sigma(\gamma + \mathrm{p} \to J/\psi + \mathrm{p})$ reported in Table III as a function of $W_{\gamma\mathrm{p}}$, covering the range $27 < W_{\gamma\mathrm{p}} < 57$ GeV. Comparisons with previous measurements and with several theoretical models are also shown.

Measurements at low $W_{\gamma\mathrm{p}}$ were performed by fixed target experiments, such as those reported by the E401 [66], E516 [67], and E687 [68] Collaborations. Recently, measurements were performed near threshold by the GlueX Collaboration [72] and by the E12-16-007 experiment [73] which are not shown in Fig. 6 since they fall outside of the power-law applicability discussed below.

The cross sections are also compared with previous ALICE results in p-Pb at $\sqrt{s_{\mathrm{NN}}} = 5.02$ TeV [14,69], at forward, mid, and backward rapidity, covering the energy range $21 < W_{\gamma\mathrm{p}} < 952$ GeV.

In this analysis, a χ^2 fit of a power-law function, $N(W_{\gamma\mathrm{p}}/W_0)^{\delta}$, is performed to the two ALICE datasets at $\sqrt{s_{\mathrm{NN}}} = 8.16$ and $\sqrt{s_{\mathrm{NN}}} = 5.02$ TeV together, with $W_0 = 90.0$ GeV, as done in HERA analyses [38–40] and for

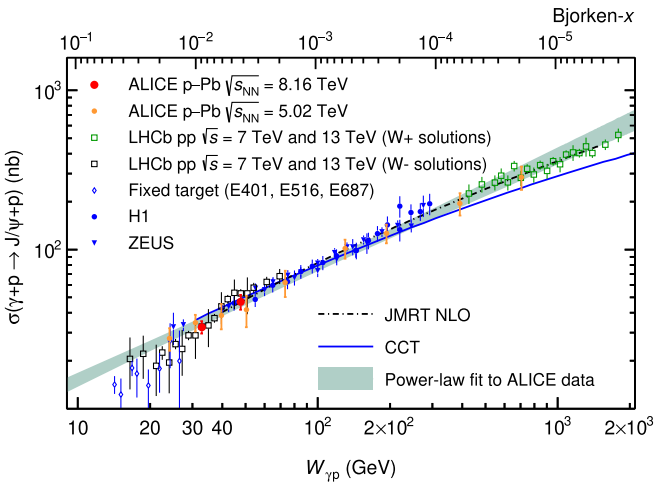

FIG. 6. Exclusive J/ψ photoproduction cross section off protons measured as a function of the center-of-mass energy of the photon-proton system $W_{\gamma\mathrm{p}}$ by ALICE in p-Pb UPCs and compared with previous measurements [14,38–40,43–45,66–69] and with next-to-leading-order JMRT [70,71] and CCT [37] models. The power-law fit to the ALICE data is also shown. The uncertainties of the data points are the quadratic sum of the statistical and systematic uncertainties.

previous ALICE measurements [14]. The technique follows what was done by the H1 Collaboration [74] and the fit takes into account the statistical and systematic uncertainties. The parameters obtained from the fit are $N = 71.6 \pm 3.7$ nb and $\delta = 0.70 \pm 0.04$ with a correlation of $+0.16$ between the two parameters. The quality of the fit is $\chi^2/\mathrm{ndf} = 1.62$ for 9 degrees of freedom. The value of the exponent is the same as in previous ALICE measurements [14]. The H1 and ZEUS measurements, performed over an energy range $W_{\gamma p}$ that encompasses the new ALICE measurements, are also shown in the same figure. They, respectively, found $\delta = 0.69 \pm 0.02(\mathrm{stat}) \pm 0.03(\mathrm{syst})$ and $\delta = 0.67 \pm 0.03(\mathrm{tot})$ [38–40]. Thus, the measurements by ALICE are compatible with the values measured by HERA experiments, and no deviation from a power law is observed up to about 700 GeV.

LHCb measured the exclusive J/ψ photoproduction cross sections in pp collisions, at $\sqrt{s_{\mathrm{NN}}} = 7$ TeV [43,44] and 13 TeV [45]. The LHCb analyses use data from a symmetric system and thus suffer from the ambiguity in identifying the photon emitter and the photon target. Since the nonexclusive J/ψ photoproduction depends on $W_{\gamma p}$, these processes are difficult to subtract and make the extraction of the underlying $\sigma(W_{\gamma p})$ strongly model dependent. Moreover, the uncertainty in the hadronic survival probability in pp collisions is much larger than in p-Pb collisions, and samples of pp collisions can contain a contamination of J/ψ production through Odderon-Pomeron fusion [30,75]. For each $\mathrm{d}\sigma/\mathrm{d}y$ measurement, LHCb reported two solutions, one for low $W_{\gamma p}$ and one for high $W_{\gamma p}$. Despite these ambiguities and assumptions, the LHCb solutions are found to be compatible with ALICE measurements within the current uncertainties.

ALICE measurements are also compared with the Jones-Martin-Ryskin-Teubner (JMRT) calculation. Two calculations are available from the JMRT group [70,71]. The first one, referred to as LO, is based on a power-law description of the process from the result in Ref. [32], while the second one, labeled as NLO, includes contributions which mimic effects expected from the dominant NLO corrections. At high $W_{\gamma p}$, they deviate from a simple power-law shape. Both models are fitted to the same data and their energy dependence is rather similar, so only the NLO version is shown. ALICE measurements at $\sqrt{s_{\mathrm{NN}}} = 5.02$ and $\sqrt{s_{\mathrm{NN}}} = 8.16$ TeV support their extracted gluon distribution down to $x \sim 2 \times 10^{-5}$. A more recent NLO computation of this process suggests a stronger sensitivity to quark contributions than previously considered [33].

Figure 6 also shows predictions from the Cepila-Contreras-Takaki (CCT) model [37] based on the color dipole approach. This model incorporates a fluctuating hot spot structure of the proton in the impact parameter plane, with the number of hot spots growing with decreasing x. It is compatible with ALICE measurements at $\sqrt{s_{\mathrm{NN}}} = 5.02$ and $\sqrt{s_{\mathrm{NN}}} = 8.16$ TeV. Future UPC measurements by ALICE will explore the high W range, particularly with future detector upgrades such as FoCal [76].

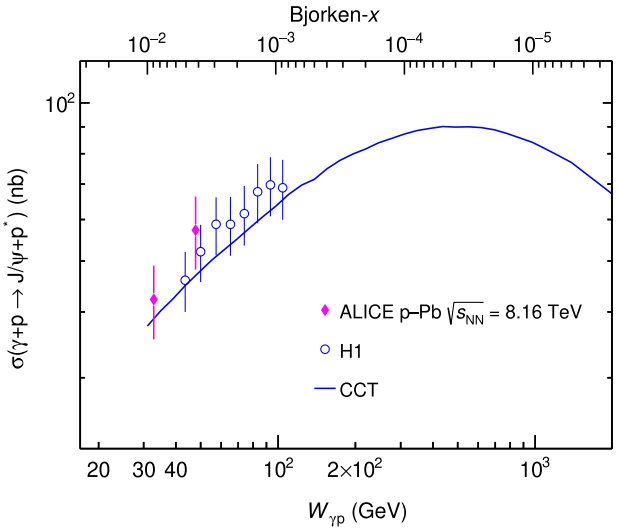

FIG. 7. Dissociative J/ψ photoproduction cross section off protons measured by ALICE in p-Pb UPCs at $\sqrt{s_{\mathrm{NN}}} = 8.16$ TeV and compared with H1 data [40]. A comparison with the CCT model [37] is shown. The uncertainties of the data points are the quadratic sum of the statistical and systematic uncertainties.

2. Dissociative J/ψ photoproduction

Figure 7 shows the ALICE measurement of the dissociative J/ψ photoproduction cross section $\sigma(\gamma + \mathrm{p} \to J/\psi + \mathrm{p}^{(*)})$ as a function of $W_{\gamma p}$, covering the range $27 < W_{\gamma p} < 57$ GeV. The cross sections are also reported in Table III. A previous measurement at similar energies by H1 [40] is also shown and is in good agreement with the ALICE measurement. In addition, the experimental results are compared with the CCT model [37] discussed in the previous section. In the framework of this model, the exclusive cross section is sensitive to the average interaction of the color dipole $\mathrm{q\bar{q}}$ with the proton, and the dissociative cross section is sensitive to the fluctuations in the $\mathrm{q\bar{q}}$-proton interaction between the different color field configurations of the proton. The model describes correctly the energy evolution of the dissociative cross section both for H1 and ALICE measurements and predicts that the cross section will reach a maximum at $W_{\gamma p} \simeq 500$ GeV, then decrease at higher energies. This behavior is expected due to the hot spots saturating the proton area.

3. Ratio of dissociative-to-exclusive J/ψ photoproduction

ALICE measurements for the ratio of dissociative-to-exclusive J/ψ photoproduction cross sections, $\sigma(\gamma + \mathrm{p} \to J/\psi + \mathrm{p}^{(*)})/\sigma(\gamma + \mathrm{p} \to J/\psi + \mathrm{p})$, are given in Table IV.

TABLE IV. Ratio of dissociative-to-exclusive J/ψ photoproduction cross sections in p-Pb UPCs at $\sqrt{s_{\rm NN}} = 8.16$ TeV. The first uncertainty is the statistical one. Its size is strongly impacted by the anticorrelation between exclusive and dissociative J/ψ components in the two-dimensional fit. The second uncertainty is the systematic one. It is computed as the quadratic sum of the signal extraction ratio uncertainty and the uncertainty on the V0C veto.

Rapidity range	$W_{\gamma p}$ (GeV)	$\langle W_{\gamma p} \rangle$ (GeV)	$\frac{\sigma(\gamma+p\to J/\psi+p^{(*)})}{\sigma(\gamma+p\to J/\psi+p)}$
(2.5, 4)	(27, 57)	39.9	$1.27 \pm 0.15 \pm 0.18$
(3.25, 4)	(27, 39)	32.8	$1.29 \pm 0.23 \pm 0.19$
(2.5, 3.25)	(39, 57)	47.7	$1.21 \pm 0.18 \pm 0.18$

These measurements are also shown in Fig. 8 as a function of $W_{\gamma p}$, together with the measurements by H1 [40] at similar energies. Two models are compared with the measurements: the CCT model [37] and a model calculation by Mäntysaari-Schenke [77]. The MS model is based on the perturbative Jalilian–Iancu–McLerran–Weigert–Leonidov–Kovner (JIMWLK) evolution [78,79], with initial parameters constrained from fits to H1 data starting from $x \sim 10^{-3}$. At high $W_{\gamma p}$, where the gluon saturation regime is expected, the models predict that the ratio of dissociative-to-exclusive cross sections vanishes.

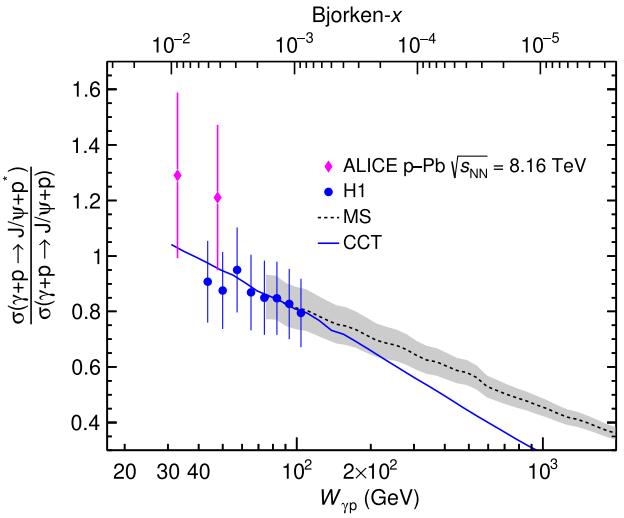

FIG. 8. Ratio of dissociative-to-exclusive J/ψ photoproduction cross sections measured by ALICE in p-Pb UPCs at $\sqrt{s_{\rm NN}} = 8.16$ TeV and compared with H1 measurements [40]. The uncertainties of the data points are the quadratic sum of the statistical and systematic uncertainties. The experimental uncertainties for the H1 data are computed assuming completely independent uncertainties for the exclusive and dissociative cross sections. The measurements are compared with the CCT model [37] and a model by Mäntysaari-Schenke (MS) [77]. The uncertainty band of the MS model corresponds to the statistical uncertainty of the calculation.

VII. SUMMARY

This article presents three different measurements carried out by the ALICE Collaboration in ultraperipheral p-Pb collisions at $\sqrt{s_{\rm NN}} = 8.16$ TeV. The exclusive dimuon continuum production from two-photon interactions in the invariant mass range from 1 to 2.5 GeV/c^2 is presented. It is compared with STARlight and SuperChic and found to be compatible within 3 standard deviations. Since these models are based on LO QED calculations, this measurement can be used to provide a limit on higher-order corrections for this process. Furthermore, the exclusive and dissociative J/ψ photoproductions off protons were measured. The measurement of exclusive J/ψ photoproduction cross section is compared with those previously performed by ALICE, LHCb, H1, and ZEUS Collaborations. The ALICE measurements are consistent with a power-law dependence on $W_{\gamma p}$ of $\sigma(\gamma p \to J/\psi p)$, with the power found to be $\delta = 0.70 \pm 0.04$. The measurement of the cross section of dissociative photoproduction of J/ψ mesons is the first of its kind at the LHC and a first measurement of this type at a hadron collider. It is in good agreement with H1 measurements. This is the first step to probe the fluctuation of the subnucleonic structure in protons in ultraperipheral collisions at high energies.

ACKNOWLEDGMENTS

The ALICE Collaboration would like to thank all its engineers and technicians for their invaluable contributions to the construction of the experiment and the CERN accelerator teams for the outstanding performance of the LHC complex. The ALICE Collaboration gratefully acknowledges the resources and support provided by all grid centers and the Worldwide LHC Computing Grid (WLCG) Collaboration. The ALICE Collaboration acknowledges the following funding agencies for their support in building and running the ALICE detector: A. I. Alikhanyan National Science Laboratory (Yerevan Physics Institute) Foundation (ANSL), State Committee of Science and World Federation of Scientists (WFS), Armenia; Austrian Academy of Sciences, Austrian Science Fund (FWF): [M 2467-N36], and Nationalstiftung für Forschung, Technologie und Entwicklung, Austria; Ministry of Communications and High Technologies, National Nuclear Research Center, Azerbaijan; Conselho Nacional de Desenvolvimento Científico e Tecnológico (CNPq), Financiadora de Estudos e Projetos (Finep), Fundação de Amparo à Pesquisa do Estado de São Paulo (FAPESP), and Universidade Federal do Rio Grande do Sul (UFRGS), Brazil; Bulgarian Ministry of Education and Science, within the National Roadmap for Research Infrastructures 2020-2027 (object CERN), Bulgaria; Ministry of Education of China (MOEC), Ministry of Science and Technology of China (MSTC),

and National Natural Science Foundation of China (NSFC), China; Ministry of Science and Education and Croatian Science Foundation, Croatia; Centro de Aplicaciones Tecnológicas y Desarrollo Nuclear (CEADEN), Cubaenergía, Cuba; Ministry of Education, Youth and Sports of the Czech Republic, Czech Republic; The Danish Council for Independent Research | Natural Sciences, the VILLUM FONDEN, and Danish National Research Foundation (DNRF), Denmark; Helsinki Institute of Physics (HIP), Finland; Commissariat à l'Energie Atomique (CEA) and Institut National de Physique Nucléaire et de Physique des Particules (IN2P3) and Centre National de la Recherche Scientifique (CNRS), France; Bundesministerium für Bildung und Forschung (BMBF) and GSI Helmholtzzentrum für Schwerionenforschung GmbH, Germany; General Secretariat for Research and Technology, Ministry of Education, Research and Religions, Greece; National Research, Development and Innovation Office, Hungary; Department of Atomic Energy Government of India (DAE), Department of Science and Technology, Government of India (DST), University Grants Commission, Government of India (UGC), and Council of Scientific and Industrial Research (CSIR), India; National Research and Innovation Agency—BRIN, Indonesia; Istituto Nazionale di Fisica Nucleare (INFN), Italy; Japanese Ministry of Education, Culture, Sports, Science and Technology (MEXT) and Japan Society for the Promotion of Science (JSPS) KAKENHI, Japan; Consejo Nacional de Ciencia (CONACYT) y Tecnología, through Fondo de Cooperación Internacional en Ciencia y Tecnología (FONCICYT) and Dirección General de Asuntos del Personal Academico (DGAPA), Mexico; Nederlandse Organisatie voor Wetenschappelijk Onderzoek (NWO), Netherlands; The Research Council of Norway, Norway; Commission on Science and Technology for Sustainable Development in the South (COMSATS), Pakistan; Pontificia Universidad Católica del Perú, Peru; Ministry of Education and Science, National Science Centre, and WUT ID-UB, Poland; Korea Institute of Science and Technology Information and National Research Foundation of Korea (NRF), Republic of Korea; Ministry of Education and Scientific Research, Institute of Atomic Physics, Ministry of Research and Innovation and Institute of Atomic Physics, and University Politehnica of Bucharest, Romania; Ministry of Education, Science, Research and Sport of the Slovak Republic, Slovakia; National Research Foundation of South Africa, South Africa; Swedish Research Council (VR) and Knut and Alice Wallenberg Foundation (KAW), Sweden; European Organization for Nuclear Research, Switzerland; Suranaree University of Technology (SUT), National Science and Technology Development Agency (NSTDA), Thailand Science Research and Innovation (TSRI), and National Science, Research and Innovation Fund (NSRF), Thailand; Turkish Energy, Nuclear and Mineral Research Agency (TENMAK), Turkey; National Academy of Sciences of Ukraine, Ukraine; Science and Technology Facilities Council (STFC), United Kingdom; National Science Foundation (NSF) and U.S. Department of Energy, Office of Nuclear Physics (DOE NP), USA. In addition, individual groups or members have received support from: European Research Council, Strong 2020—Horizon 2020 (Grants No. 950692, No. 824093), European Union; Academy of Finland (Center of Excellence in Quark Matter) (Grant No. 346327, No. 346328), Finland; Programa de Apoyos para la Superación del Personal Académico, UNAM, Mexico. This work is supported in part in the framework of the GLUODYNAMICS project funded by the "P2IO LabEx (ANR-10-LABX-0038)" in the framework "Investissements d'Avenir" (ANR-11-IDEX-0003-01) managed by the Agence Nationale de la Recherche (ANR), France.

[1] A. J. Baltz, The physics of ultraperipheral collisions at the LHC, Phys. Rep. **458**, 1 (2008).

[2] J. G. Contreras and J. D. Tapia Takaki, Ultra-peripheral heavy-ion collisions at the LHC, Int. J. Mod. Phys. A **30**, 1542012 (2015).

[3] S. Klein and P. Steinberg, Photonuclear and two-photon interactions at high-energy nuclear colliders, Annu. Rev. Nucl. Part. Sci. **70**, 323 (2020).

[4] D. d'Enterria and G. G. da Silveira, Observing light-by-light scattering at the Large Hadron Collider, Phys. Rev. Lett. **111**, 080405 (2013); **116**, 129901(E) (2016).

[5] M. Kłusek-Gawenda, P. Lebiedowicz, and A. Szczurek, Light-by-light scattering in ultraperipheral Pb-Pb collisions at energies available at the CERN Large Hadron Collider, Phys. Rev. C **93**, 044907 (2016).

[6] G. Aad *et al.* (ATLAS Collaboration), Observation of light-by-light scattering in ultraperipheral Pb + Pb collisions with the ATLAS detector, Phys. Rev. Lett. **123**, 052001 (2019).

[7] G. Aad *et al.* (ATLAS Collaboration), Measurement of light-by-light scattering and search for axion-like particles with 2.2 nb^{-1} of Pb + Pb data with the ATLAS detector, J. High Energy Phys. 11 (**2021**) 050.

[8] M. Aaboud *et al.* (ATLAS Collaboration), Evidence for light-by-light scattering in heavy-ion collisions with the ATLAS detector at the LHC, Nat. Phys. **13**, 852 (2017).

[9] A. M. Sirunyan *et al.* (CMS Collaboration), Evidence for light-by-light scattering and searches for axion-like particles in ultraperipheral Pb-Pb collisions at $\sqrt{s_{\mathrm{NN}}} = 5.02$ TeV, Phys. Lett. B **797**, 134826 (2019).

[10] W. Zha and Z. Tang, Discovery of higher-order quantum electrodynamics effect for the vacuum pair production, J. High Energy Phys. 08 (**2021**) 083.

[11] K. Hencken, E. A. Kuraev, and V. Serbo, Exclusive and inclusive muon pair production in collisions of relativistic nuclei, Phys. Rev. C **75**, 034903 (2007).

[12] A. J. Baltz and J. Nystrand, Higher order QED in high mass e^+e^- pairs production at RHIC, Phys. Rev. C **82**, 027901 (2010).

[13] E. Abbas *et al.* (ALICE Collaboration), Charmonium and e^+e^- pair photoproduction at mid-rapidity in ultra-peripheral Pb-Pb collisions at $\sqrt{s_{\mathrm{NN}}} = 2.76$ TeV, Eur. Phys. J. C **73**, 2617 (2013).

[14] S. Acharya *et al.* (ALICE Collaboration), Energy dependence of exclusive J/ψ photoproduction off protons in ultra-peripheral p-Pb collisions at $\sqrt{s_{\mathrm{NN}}} = 5.02$ TeV, Eur. Phys. J. C **79**, 402 (2019).

[15] A. M. Sirunyan *et al.* (CMS Collaboration), Observation of forward neutron multiplicity dependence of dimuon acoplanarity in ultraperipheral Pb-Pb collisions at $\sqrt{s_{\mathrm{NN}}} = 5.02$ TeV, Phys. Rev. Lett. **127**, 122001 (2021).

[16] G. Aad *et al.* (ATLAS Collaboration), Measurement of muon pairs produced via $\gamma\gamma$ scattering in non-ultraperipheral Pb + Pb collisions at $\sqrt{s_{\mathrm{NN}}} = 5.02$ TeV with the ATLAS detector, Phys. Rev. C **107**, 054907 (2023).

[17] S. Afanasiev *et al.* (PHENIX Collaboration), Photoproduction of J/ψ and of high mass e^+e^- in ultra-peripheral Au + Au collisions at $\sqrt{s_{\mathrm{NN}}} = 200$ GeV, Phys. Lett. B **679**, 321 (2009).

[18] J. Adams *et al.* (STAR Collaboration), Production of e^+e^- pairs accompanied by nuclear dissociation in ultra-peripheral heavy ion collision, Phys. Rev. C **70**, 031902 (2004).

[19] J. Adam *et al.* (STAR Collaboration), Measurement of e^+e^- momentum and angular distributions from linearly polarized photon collisions, Phys. Rev. Lett. **127**, 052302 (2021).

[20] J. Adam *et al.* (STAR Collaboration), Low-p_T e^+e^- pair production in Au + Au collisions at $\sqrt{s_{NN}} = 200$ GeV and U + U collisions at $\sqrt{s_{NN}} = 193$ GeV at STAR, Phys. Rev. Lett. **121**, 132301 (2018).

[21] G. Aad *et al.* (ATLAS Collaboration), Exclusive dimuon production in ultraperipheral Pb + Pb collisions at $\sqrt{s_{NN}} = 5.02$ TeV with ATLAS, Phys. Rev. C **104**, 024906 (2021).

[22] S. R. Klein, J. Nystrand, J. Seger, Y. Gorbunov, and J. Butterworth, STARlight: A Monte Carlo simulation program for ultra-peripheral collisions of relativistic ions, Comput. Phys. Commun. **212**, 258 (2017).

[23] L. A. Harland-Lang, V. A. Khoze, and M. G. Ryskin, Elastic photon-initiated production at the LHC: The role of hadron-hadron interactions, SciPost Phys. **11**, 064 (2021).

[24] N. Burmasov, E. Kryshen, P. Buehler, and R. Lavicka, Upcgen: A Monte Carlo simulation program for dilepton pair production in ultra-peripheral collisions of heavy ions, Comput. Phys. Commun. **277**, 108388 (2022).

[25] C. Azevedo, V. P. Gonçalves, and B. D. Moreira, Exclusive dilepton production in ultraperipheral Pb-Pb collisions at the LHC, Eur. Phys. J. C **79**, 432 (2019).

[26] G. Aad *et al.* (ATLAS Collaboration), Measurement of exclusive $\gamma\gamma \to \ell^+\ell^-$ production in proton-proton collisions at $\sqrt{s} = 7$ TeV with the ATLAS detector, Phys. Lett. B **749**, 242 (2015).

[27] M. Aaboud *et al.* (ATLAS Collaboration), Measurement of the exclusive $\gamma\gamma \to \mu^+\mu^-$ process in proton-proton collisions at $\sqrt{s} = 13$ TeV with the ATLAS detector, Phys. Lett. B **777**, 303 (2018).

[28] S. Chatrchyan *et al.* (CMS Collaboration), Exclusive photon-photon production of muon pairs in proton–proton collisions at $\sqrt{s} = 7$ TeV, J. High Energy Phys. 01 (2012) 052.

[29] A. Abulencia *et al.* (CDF Collaboration), Observation of exclusive electron-positron production in hadron-hadron collisions, Phys. Rev. Lett. **98**, 112001 (2007).

[30] T. Aaltonen *et al.* (CDF Collaboration), Observation of exclusive charmonium production and $\gamma + \gamma$ to $\mu^+\mu^-$ in $p\bar{p}$ collisions at $\sqrt{s} = 1.96$ TeV, Phys. Rev. Lett. **102**, 242001 (2009).

[31] P. Newman and M. Wing, The hadronic final state at HERA, Rev. Mod. Phys. **86**, 1037 (2014).

[32] M. G. Ryskin, Diffractive J/ψ electroproduction in LLA QCD, Z. Phys. C **57**, 89 (1993).

[33] K. J. Eskola, C. A. Flett, V. Guzey, T. Löytäinen, and H. Paukkunen, Exclusive J/ψ photoproduction in ultraperipheral Pb + Pb collisions at the CERN Large Hadron Collider calculated at next-to-leading order perturbative QCD, Phys. Rev. C **106**, 035202 (2022).

[34] A. Morreale and F. Salazar, Mining for gluon saturation at colliders, Universe **7**, 312 (2021).

[35] H. I. Miettinen and J. Pumplin, Diffraction scattering and the parton structure of hadrons, Phys. Rev. D **18**, 1696 (1978).

[36] H. Mäntysaari, Review of proton and nuclear shape fluctuations at high energy, Rep. Prog. Phys. **83**, 082201 (2020).

[37] J. Cepila, J. G. Contreras, and J. D. Tapia Takaki, Energy dependence of dissociative J/ψ photoproduction as a signature of gluon saturation at the LHC, Phys. Lett. B **766**, 186 (2017).

[38] S. Chekanov *et al.* (ZEUS Collaboration), Exclusive photoproduction of J/ψ mesons at HERA, Eur. Phys. J. C **24**, 345 (2002).

[39] A. Aktas *et al.* (H1 Collaboration), Elastic J/ψ production at HERA, Eur. Phys. J. C **46**, 585 (2006).

[40] C. Alexa *et al.* (H1 Collaboration), Elastic and proton-dissociative photoproduction of J/ψ mesons at HERA, Eur. Phys. J. C **73**, 2466 (2013).

[41] S. Chekanov *et al.* (ZEUS Collaboration), Measurement of J/ψ photoproduction at large momentum transfer at HERA, J. High Energy Phys. 05 (2010) 085.

[42] B. Abelev *et al.* (ALICE Collaboration), Exclusive J/ψ photoproduction off protons in ultra-peripheral p-Pb collisions at $\sqrt{s_{\mathrm{NN}}} = 5.02$ TeV, Phys. Rev. Lett. **113**, 232504 (2014).

[43] R. Aaij *et al.* (LHCb Collaboration), Exclusive J/ψ and $\psi(2S)$ production in pp collisions at $\sqrt{s} = 7$ TeV, J. Phys. G **40**, 045001 (2013).

[44] R. Aaij *et al.* (LHCb Collaboration), Updated measurements of exclusive J/ψ and $\psi(2S)$ production cross-sections in pp collisions at $\sqrt{s} = 7$ TeV, J. Phys. G **41**, 055002 (2014).

[45] R. Aaij *et al.* (LHCb Collaboration), Central exclusive production of J/ψ and $\psi(2S)$ mesons in pp collisions at $\sqrt{s} = 13$ TeV, J. High Energy Phys. 10 (2018) 167.

[46] K. Aamodt *et al.* (ALICE Collaboration), The ALICE experiment at the CERN LHC, J. Instrum. **3**, S08002 (2008).

[47] B. Abelev *et al.* (ALICE Collaboration), Performance of the ALICE experiment at the CERN LHC, Int. J. Mod. Phys. A **29**, 1430044 (2014).

[48] K. Aamodt *et al.* (ALICE Collaboration), Rapidity and transverse momentum dependence of inclusive J/ψ production in pp collisions at $\sqrt{s} = 7$ TeV, Phys. Lett. B **704**, 442 (2011); **718**, 692(E) (2012).

[49] K. Akiba *et al.*, LHC forward physics, J. Phys. G **43**, 110201 (2016).

[50] M. Broz *et al.*, Performance of ALICE AD modules in the CERN PS test beam, J. Instrum. **16**, P01017 (2021).

[51] A. Alici *et al.*, Study of the LHC ghost charge and satellite bunches for luminosity calibration, https://cds.cern.ch/record/1427728.

[52] S. Acharya *et al.* (ALICE Collaboration), ALICE luminosity determination for p-Pb collisions at $\sqrt{s_{\rm NN}} = 8.16$ TeV, Report No. ALICE-PUBLIC-2018-002, 2018, https://cds.cern.ch/record/2314660.

[53] H. Jung, Hard diffractive scattering in high-energy e p collisions and the Monte Carlo generator RAPGAP, Comput. Phys. Commun. **86**, 147 (1995).

[54] S. Klein and J. Nystrand, Exclusive vector meson production in relativistic heavy ion collisions, Phys. Rev. C **60**, 014903 (1999).

[55] R. Brun, F. Bruyant, F. Carminati, S. Giani, M. Maire, A. McPherson, G. Patrick, and L. Urban, *GEANT: Detector Description and Simulation Tool; 1994*, CERN Program Library (CERN, Geneva, 1993), https://cds.cern.ch/record/1082634.

[56] J. E. Gaiser, Charmonium spectroscopy from radiative decays of the J/ψ and ψ', Ph.D. thesis, Stanford Linear Accelerator Center, 1982, https://www.osti.gov/biblio/6237411.

[57] J. Adam *et al.* (ALICE Collaboration), Quarkonium signal extraction in ALICE, Report No. ALICE-PUBLIC-2015-006, https://cds.cern.ch/record/2060096.

[58] M. Pivk and F. R. Le Diberder, SPlot: A statistical tool to unfold data distributions, Nucl. Instrum. Methods Phys. Res., Sect. A **555**, 356 (2005).

[59] S. Acharya *et al.* (ALICE Collaboration), Coherent J/ψ photoproduction at forward rapidity in ultra-peripheral Pb-Pb collisions at $\sqrt{s_{\rm NN}} = 5.02$ TeV, Phys. Lett. B **798**, 134926 (2019).

[60] P. D. Group, Review of particle physics, Prog. Theor. Exp. Phys. **2020**, 083C01 (2020).

[61] C. Adloff *et al.* (H1 Collaboration), Diffractive photoproduction of $\psi(2S)$ mesons at HERA, Phys. Lett. B **541**, 251 (2002).

[62] J. Z. Bai *et al.* (BES Collaboration), $\psi(2S) \to \pi^+\pi^- J/\psi$ decay distributions, Phys. Rev. D **62**, 032002 (2000).

[63] S. Acharya *et al.* (ALICE Collaboration), Inclusive J/ψ production at forward and backward rapidity in p-Pb collisions at $\sqrt{s_{\rm NN}} = 8.16$ TeV, J. High Energy Phys. 07 (2018) 160.

[64] L. A. Harland-Lang, M. Tasevsky, V. A. Khoze, and M. G. Ryskin, A new approach to modelling elastic and inelastic photon-initiated production at the LHC: SuperChic 4, Eur. Phys. J. C **80**, 925 (2020).

[65] L. A. Harland-Lang, V. A. Khoze, and M. G. Ryskin, Exclusive LHC physics with heavy ions: SuperChic 3, Eur. Phys. J. C **79**, 39 (2019).

[66] M. E. Binkley *et al.*, J/ψ photoproduction from 60 to 300 GeV/c, Phys. Rev. Lett. **48**, 73 (1982).

[67] B. Denby *et al.*, Inelastic and elastic photoproduction of J/ψ (3097), Phys. Rev. Lett. **52**, 795 (1984).

[68] P. Frabetti *et al.* (E687 Collaboration), A measurement of elastic J/ψ photoproduction cross section at FermiLab E687, Phys. Lett. B **316**, 197 (1993).

[69] B. Abelev *et al.* (ALICE Collaboration), Exclusive J/ψ photoproduction off protons in ultraperipheral p-Pb collisions at $\sqrt{s_{\rm NN}} = 5.02$ TeV, Phys. Rev. Lett. **113**, 232504 (2014).

[70] S. P. Jones, A. D. Martin, M. G. Ryskin, and T. Teubner, Probes of the small-x gluon via exclusive J/ψ and Υ production at HERA and the LHC, J. High Energy Phys. 11 (2013) 085.

[71] S. P. Jones, A. D. Martin, M. G. Ryskin, and T. Teubner, Exclusive J/ψ production at the LHC in the k_T factorization approach, J. Phys. G **44**, 03LT01 (2017).

[72] A. Ali *et al.* (GlueX Collaboration), First measurement of near-threshold J/ψ exclusive photoproduction off the proton, Phys. Rev. Lett. **123**, 072001 (2019).

[73] B. Duran *et al.*, Determining the gluonic gravitational form factors of the proton, Nature (London) **615**, 813 (2023).

[74] F. D. Aaron *et al.* (H1 Collaboration), Measurement of the inclusive ep scattering cross section at low Q^2 and x at HERA, Eur. Phys. J. C **63**, 625 (2009).

[75] A. J. Schramm and D. H. Reeves, Production of η mesons in double pomeron exchange, Phys. Rev. D **55**, 7312 (1997).

[76] A. Bylinkin, J. Nystrand, and D. Tapia Takaki, Vector meson photoproduction in UPCs with FoCal, J. Phys. G, **50**, 055105 (2023).

[77] H. Mäntysaari and B. Schenke, Confronting impact parameter dependent JIMWLK evolution with HERA data, Phys. Rev. D **98**, 034013 (2018).

[78] J. Jalilian-Marian, A. Kovner, L. D. McLerran, and H. Weigert, The intrinsic glue distribution at very small x, Phys. Rev. D **55**, 5414 (1997).

[79] J. Jalilian-Marian, A. Kovner, A. Leonidov, and H. Weigert, The BFKL equation from the Wilson renormalization group, Nucl. Phys. **B504**, 415 (1997).

S. Acharya,[125] D. Adamová,[86] A. Adler,[69] G. Aglieri Rinella,[32] M. Agnello,[29] N. Agrawal,[50] Z. Ahammed,[132] S. Ahmad,[15] S. U. Ahn,[70] I. Ahuja,[37] A. Akindinov,[140] M. Al-Turany,[97] D. Aleksandrov,[140] B. Alessandro,[55] H. M. Alfanda,[6] R. Alfaro Molina,[66] B. Ali,[15] A. Alici,[25a,25b] N. Alizadehvandchali,[114] A. Alkin,[32] J. Alme,[20]

G. Alocco,[51] T. Alt,[63] I. Altsybeev,[140] M. N. Anaam,[6] C. Andrei,[45] A. Andronic,[135] V. Anguelov,[94] F. Antinori,[53] P. Antonioli,[50] N. Apadula,[74] L. Aphecetche,[103] H. Appelshäuser,[63] C. Arata,[73] S. Arcelli,[25a,25b] M. Aresti,[51] R. Arnaldi,[55] J. G. M. C. A. Arneiro,[110] I. C. Arsene,[19] M. Arslandok,[137] A. Augustinus,[32] R. Averbeck,[97] M. D. Azmi,[15] A. Badalà,[52] J. Bae,[104] Y. W. Baek,[40] X. Bai,[118] R. Bailhache,[63] Y. Bailung,[47] A. Balbino,[29] A. Baldisseri,[128] B. Balis,[2] D. Banerjee,[4a,4b] Z. Banoo,[91] R. Barbera,[26a,26b] F. Barile,[31a,31b] L. Barioglio,[95] M. Barlou,[78] G. G. Barnaföldi,[136] L. S. Barnby,[85] V. Barret,[125] L. Barreto,[110] C. Bartels,[117] K. Barth,[32] E. Bartsch,[63] N. Bastid,[125] S. Basu,[75] G. Batigne,[103] D. Battistini,[95] B. Batyunya,[141] D. Bauri,[46] J. L. Bazo Alba,[101] I. G. Bearden,[83] C. Beattie,[137] P. Becht,[97] D. Behera,[47] I. Belikov,[127] A. D. C. Bell Hechavarria,[135] F. Bellini,[25a,25b] R. Bellwied,[114] S. Belokurova,[140] G. Bencedi,[136] S. Beole,[24a,24b] A. Bercuci,[45] Y. Berdnikov,[140] A. Berdnikova,[94] L. Bergmann,[94] M. G. Besoiu,[62] L. Betev,[32] P. P. Bhaduri,[132] A. Bhasin,[91] M. A. Bhat,[4a,4b] B. Bhattacharjee,[41] L. Bianchi,[24a,24b] N. Bianchi,[48] J. Bielčík,[35] J. Bielčíková,[86] J. Biernat,[107] A. P. Bigot,[127] A. Bilandzic,[95] G. Biro,[136] S. Biswas,[4a,4b] N. Bize,[103] J. T. Blair,[108] D. Blau,[140] M. B. Blidaru,[97] N. Bluhme,[38] C. Blume,[63] G. Boca,[21,54] F. Bock,[87] T. Bodova,[20] A. Bogdanov,[140] S. Boi,[22a,22b] J. Bok,[57] L. Boldizsár,[136] M. Bombara,[37] P. M. Bond,[32] G. Bonomi,[54,131] H. Borel,[128] A. Borissov,[140] A. G. Borquez Carcamo,[94] H. Bossi,[137] E. Botta,[24a,24b] Y. E. M. Bouziani,[63] L. Bratrud,[63] P. Braun-Munzinger,[97] M. Bregant,[110] M. Broz,[35] G. E. Bruno,[31a,31b,96] M. D. Buckland,[23a,23b] D. Budnikov,[140] H. Buesching,[63] S. Bufalino,[29] P. Buhler,[102] Z. Buthelezi,[67,121] A. Bylinkin,[20] S. A. Bysiak,[107] M. Cai,[6] H. Caines,[137] A. Caliva,[28a,28b] E. Calvo Villar,[101] J. M. M. Camacho,[109] P. Camerini,[23a,23b] F. D. M. Canedo,[110] M. Carabas,[124] A. A. Carballo,[32] F. Carnesecchi,[32] R. Caron,[126] L. A. D. Carvalho,[110] J. Castillo Castellanos,[128] F. Catalano,[24a,24b,32] C. Ceballos Sanchez,[141] I. Chakaberia,[74] P. Chakraborty,[46] S. Chandra,[132] S. Chapeland,[32] M. Chartier,[117] S. Chattopadhyay,[132] S. Chattopadhyay,[99] T. G. Chavez,[44] T. Cheng,[6,97] C. Cheshkov,[126] B. Cheynis,[126] V. Chibante Barroso,[32] D. D. Chinellato,[111] E. S. Chizzali,[95,‡] J. Cho,[57] S. Cho,[57] P. Chochula,[32] P. Christakoglou,[84] C. H. Christensen,[83] P. Christiansen,[75] T. Chujo,[123] M. Ciacco,[29] C. Cicalo,[51] F. Cindolo,[50] M. R. Ciupek,[97] G. Clai,[50,§] F. Colamaria,[49] J. S. Colburn,[100] D. Colella,[31a,31b,96] M. Colocci,[25a,25b] G. Conesa Balbastre,[73] Z. Conesa del Valle,[72] G. Contin,[23a,23b] J. G. Contreras,[35] M. L. Coquet,[128] T. M. Cormier,[87,†] P. Cortese,[55,130] M. R. Cosentino,[112] F. Costa,[32] S. Costanza,[21,54] C. Cot,[72] J. Crkovská,[94] P. Crochet,[125] R. Cruz-Torres,[74] P. Cui,[6] A. Dainese,[53] M. C. Danisch,[94] A. Danu,[62] P. Das,[80] P. Das,[4a,4b] S. Das,[4a,4b] A. R. Dash,[135] S. Dash,[46] A. De Caro,[28a,28b] G. de Cataldo,[49] J. de Cuveland,[38] A. De Falco,[22a,22b] D. De Gruttola,[28a,28b] N. De Marco,[55] C. De Martin,[23a,23b] S. De Pasquale,[28a,28b] R. Deb,[131] S. Deb,[47] K. R. Deja,[133] R. Del Grande,[95] L. Dello Stritto,[28a,28b] W. Deng,[6] P. Dhankher,[18] D. Di Bari,[31a,31b] A. Di Mauro,[32] B. Diab,[128] R. A. Diaz,[7,141] T. Dietel,[113] Y. Ding,[6] R. Divià,[32] D. U. Dixit,[18] Ø. Djuvsland,[20] U. Dmitrieva,[140] A. Dobrin,[62] B. Dönigus,[63] J. M. Dubinski,[133] A. Dubla,[97] S. Dudi,[90] P. Dupieux,[125] M. Durkac,[106] N. Dzalaiova,[12] T. M. Eder,[135] R. J. Ehlers,[74] F. Eisenhut,[63] D. Elia,[49] B. Erazmus,[103] F. Ercolessi,[25a,25b] F. Erhardt,[89] M. R. Ersdal,[20] B. Espagnon,[72] G. Eulisse,[32] D. Evans,[100] S. Evdokimov,[140] L. Fabbietti,[95] M. Faggin,[27a,27b] J. Faivre,[73] F. Fan,[6] W. Fan,[74] A. Fantoni,[48] M. Fasel,[87] P. Fecchio,[29] A. Feliciello,[55] G. Feofilov,[140] A. Fernández Téllez,[44] L. Ferrandi,[110] M. B. Ferrer,[32] A. Ferrero,[128] C. Ferrero,[55] A. Ferretti,[24a,24b] V. J. G. Feuillard,[94] V. Filova,[35] D. Finogeev,[140] F. M. Fionda,[51] F. Flor,[114] A. N. Flores,[108] S. Foertsch,[67] I. Fokin,[94] S. Fokin,[140] E. Fragiacomo,[56] E. Frajna,[136] U. Fuchs,[32] N. Funicello,[28a,28b] C. Furget,[73] A. Furs,[140] T. Fusayasu,[98] J. J. Gaardhøje,[83] M. Gagliardi,[24a,24b] A. M. Gago,[101] C. D. Galvan,[109] D. R. Gangadharan,[114] P. Ganoti,[78] C. Garabatos,[97] J. R. A. Garcia,[44] E. Garcia-Solis,[9] C. Gargiulo,[32] K. Garner,[135] P. Gasik,[97] A. Gautam,[116] M. B. Gay Ducati,[65] M. Germain,[103] A. Ghimouz,[123] C. Ghosh,[132] M. Giacalone,[25a,25b,50] P. Giubellino,[55,97] P. Giubilato,[27a,27b] A. M. C. Glaenzer,[128] P. Glässel,[94] E. Glimos,[120] D. J. Q. Goh,[76] V. Gonzalez,[134] M. Gorgon,[2] K. Goswami,[47] S. Gotovac,[33] V. Grabski,[66] L. K. Graczykowski,[133] E. Grecka,[86] A. Grelli,[58] C. Grigoras,[32] V. Grigoriev,[140] S. Grigoryan,[1,141] F. Grosa,[32] J. F. Grosse-Oetringhaus,[32] R. Grosso,[97] D. Grund,[35] G. G. Guardiano,[111] R. Guernane,[73] M. Guilbaud,[103] K. Gulbrandsen,[83] T. Gundem,[63] T. Gunji,[122] W. Guo,[6] A. Gupta,[91] R. Gupta,[91] R. Gupta,[47] S. P. Guzman,[44] K. Gwizdziel,[133] L. Gyulai,[136] M. K. Habib,[97] C. Hadjidakis,[72] F. U. Haider,[91] H. Hamagaki,[76] A. Hamdi,[74] M. Hamid,[6] Y. Han,[138] B. G. Hanley,[134] R. Hannigan,[108] J. Hansen,[75] M. R. Haque,[133] J. W. Harris,[137] A. Harton,[9] H. Hassan,[87] D. Hatzifotiadou,[50] P. Hauer,[42]

L. B. Havener,[137] S. T. Heckel,[95] E. Hellbär,[97] H. Helstrup,[34] M. Hemmer,[63] T. Herman,[35] G. Herrera Corral,[8] F. Herrmann,[135] S. Herrmann,[126] K. F. Hetland,[34] B. Heybeck,[63] H. Hillemanns,[32] B. Hippolyte,[127] F. W. Hoffmann,[69] B. Hofman,[58] B. Hohlweger,[84] G. H. Hong,[138] M. Horst,[95] A. Horzyk,[2] Y. Hou,[6] P. Hristov,[32] C. Hughes,[120] P. Huhn,[63] L. M. Huhta,[115] T. J. Humanic,[88] A. Hutson,[114] D. Hutter,[38] R. Ilkaev,[140] H. Ilyas,[13] M. Inaba,[123] G. M. Innocenti,[32] M. Ippolitov,[140] A. Isakov,[86] T. Isidori,[116] M. S. Islam,[99] M. Ivanov,[97] M. Ivanov,[12] V. Ivanov,[140] K. E. Iversen,[75] M. Jablonski,[2] B. Jacak,[74] N. Jacazio,[25a,25b] P. M. Jacobs,[74] S. Jadlovska,[106] J. Jadlovsky,[106] S. Jaelani,[82] C. Jahnke,[111] M. J. Jakubowska,[133] M. A. Janik,[133] T. Janson,[69] M. Jercic,[89] S. Ji,[16] S. Jia,[10] A. A. P. Jimenez,[64] F. Jonas,[87] J. M. Jowett,[32,97] J. Jung,[63] M. Jung,[63] A. Junique,[32] A. Jusko,[100] M. J. Kabus,[32,133] J. Kaewjai,[105] P. Kalinak,[59] A. S. Kalteyer,[97] A. Kalweit,[32] V. Kaplin,[140] A. Karasu Uysal,[71] D. Karatovic,[89] O. Karavichev,[140] T. Karavicheva,[140] P. Karczmarczyk,[133] E. Karpechev,[140] U. Kebschull,[69] R. Keidel,[139] D. L. D. Keijdener,[58] M. Keil,[32] B. Ketzer,[42] S. S. Khade,[47] A. M. Khan,[6,118] S. Khan,[15] A. Khanzadeev,[140] Y. Kharlov,[140] A. Khatun,[116] A. Khuntia,[107] M. B. Kidson,[113] B. Kileng,[34] B. Kim,[104] C. Kim,[16] D. J. Kim,[115] E. J. Kim,[68] J. Kim,[138] J. S. Kim,[40] J. Kim,[57] J. Kim,[68] M. Kim,[18] S. Kim,[17] T. Kim,[138] K. Kimura,[92] S. Kirsch,[63] I. Kisel,[38] S. Kiselev,[140] A. Kisiel,[133] J. P. Kitowski,[2] J. L. Klay,[5] J. Klein,[32] S. Klein,[74] C. Klein-Bösing,[135] M. Kleiner,[63] T. Klemenz,[95] A. Kluge,[32] A. G. Knospe,[114] C. Kobdaj,[105] T. Kollegger,[97] A. Kondratyev,[141] N. Kondratyeva,[140] E. Kondratyuk,[140] J. Konig,[63] S. A. Konigstorfer,[95] P. J. Konopka,[32] G. Kornakov,[133] S. D. Koryciak,[2] A. Kotliarov,[86] V. Kovalenko,[140] M. Kowalski,[107] V. Kozhuharov,[36] I. Králik,[59] A. Kravčáková,[37] L. Krcal,[32,38] M. Krivda,[59,100] F. Krizek,[86] K. Krizkova Gajdosova,[32] M. Kroesen,[94] M. Krüger,[63] D. M. Krupova,[35] E. Kryshen,[140] V. Kučera,[57] C. Kuhn,[127] P. G. Kuijer,[84] T. Kumaoka,[123] D. Kumar,[132] L. Kumar,[90] N. Kumar,[90] S. Kumar,[31a,31b] S. Kundu,[32] P. Kurashvili,[79] A. Kurepin,[140] A. B. Kurepin,[140] A. Kuryakin,[140] S. Kushpil,[86] J. Kvapil,[100] M. J. Kweon,[57] Y. Kwon,[138] S. L. La Pointe,[38] P. La Rocca,[26a,26b] A. Lakrathok,[105] M. Lamanna,[32] R. Langoy,[119] P. Larionov,[32] E. Laudi,[32] L. Lautner,[32,95] R. Lavicka,[102] R. Lea,[54,131] H. Lee,[104] I. Legrand,[45] G. Legras,[135] J. Lehrbach,[38] T. M. Lelek,[2] R. C. Lemmon,[85] I. León Monzón,[109] M. M. Lesch,[95] E. D. Lesser,[18] P. Lévai,[136] X. Li,[10] X. L. Li,[6] J. Lien,[119] R. Lietava,[100] I. Likmeta,[114] B. Lim,[24a,24b] S. H. Lim,[16] V. Lindenstruth,[38] A. Lindner,[45] C. Lippmann,[97] A. Liu,[18] D. H. Liu,[6] J. Liu,[117] G. S. S. Liveraro,[111] I. M. Lofnes,[20] C. Loizides,[87] S. Lokos,[107] J. Lomker,[58] P. Loncar,[33] J. A. Lopez,[94] X. Lopez,[125] E. López Torres,[7] P. Lu,[97,118] J. R. Luhder,[135] M. Lunardon,[27a,27b] G. Luparello,[56] Y. G. Ma,[39] M. Mager,[32] A. Maire,[127] M. V. Makariev,[36] M. Malaev,[140] G. Malfattore,[25a,25b] N. M. Malik,[91] Q. W. Malik,[19] S. K. Malik,[91] L. Malinina,[141,**] D. Mallick,[80] N. Mallick,[47] G. Mandaglio,[30,52] S. K. Mandal,[79] V. Manko,[140] F. Manso,[125] V. Manzari,[49] Y. Mao,[6] R. W. Marcjan,[2] G. V. Margagliotti,[23a,23b] A. Margotti,[50] A. Marín,[97] C. Markert,[108] P. Martinengo,[32] M. I. Martínez,[44] G. Martínez García,[103] M. P. P. Martins,[110] S. Masciocchi,[97] M. Masera,[24a,24b] A. Masoni,[51] L. Massacrier,[72] A. Mastroserio,[49,129] O. Matonoha,[75] S. Mattiazzo,[27a,27b] P. F. T. Matuoka,[110] A. Matyja,[107] C. Mayer,[107] A. L. Mazuecos,[32] F. Mazzaschi,[24a,24b] M. Mazzilli,[32] J. E. Mdhluli,[121] A. F. Mechler,[63] Y. Melikyan,[43,140] A. Menchaca-Rocha,[66] E. Meninno,[28a,28b,102] A. S. Menon,[114] M. Meres,[12] S. Mhlanga,[67,113] Y. Miake,[123] L. Micheletti,[32] L. C. Migliorin,[126] D. L. Mihaylov,[95] K. Mikhaylov,[140,141] A. N. Mishra,[136] D. Miśkowiec,[97] A. Modak,[4a,4b] A. P. Mohanty,[58] B. Mohanty,[80] M. Mohisin Khan,[15,‖] M. A. Molander,[43] Z. Moravcova,[83] C. Mordasini,[95] D. A. Moreira De Godoy,[135] I. Morozov,[140] A. Morsch,[32] T. Mrnjavac,[32] V. Muccifora,[48] S. Muhuri,[132] J. D. Mulligan,[74] A. Mulliri,[22a,22b] M. G. Munhoz,[110] R. H. Munzer,[63] H. Murakami,[122] S. Murray,[113] L. Musa,[32] J. Musinsky,[59] J. W. Myrcha,[133] B. Naik,[121] A. I. Nambrath,[18] B. K. Nandi,[46] R. Nania,[50] E. Nappi,[49] A. F. Nassirpour,[17,75] A. Nath,[94] C. Nattrass,[120] M. N. Naydenov,[36] A. Neagu,[19] A. Negru,[124] L. Nellen,[64] G. Neskovic,[38] B. S. Nielsen,[83] E. G. Nielsen,[83] S. Nikolaev,[140] S. Nikulin,[140] V. Nikulin,[140] F. Noferini,[50] S. Noh,[11] P. Nomokonov,[141] J. Norman,[117] N. Novitzky,[123] P. Nowakowski,[133] A. Nyanin,[140] J. Nystrand,[20] M. Ogino,[76] A. Ohlson,[75] V. A. Okorokov,[140] J. Oleniacz,[133] A. C. Oliveira Da Silva,[120] M. H. Oliver,[137] A. Onnerstad,[115] C. Oppedisano,[55] A. Ortiz Velasquez,[64] J. Otwinowski,[107] M. Oya,[92] K. Oyama,[76] Y. Pachmayer,[94] S. Padhan,[46] D. Pagano,[54,131] G. Paić,[64] A. Palasciano,[49] S. Panebianco,[128] H. Park,[123] H. Park,[104] J. Park,[57] J. E. Parkkila,[32] R. N. Patra,[91] B. Paul,[22a,22b] H. Pei,[6] T. Peitzmann,[58] X. Peng,[6] M. Pennisi,[24a,24b] D. Peresunko,[140] G. M. Perez,[7] S. Perrin,[128] Y. Pestov,[140] V. Petrov,[140] M. Petrovici,[45]

R. P. Pezzi,[65,103] S. Piano,[56] M. Pikna,[12] P. Pillot,[103] O. Pinazza,[32,50] L. Pinsky,[114] C. Pinto,[95] S. Pisano,[48] M. Płoskoń,[74] M. Planinic,[89] F. Pliquett,[63] M. G. Poghosyan,[87] B. Polichtchouk,[140] S. Politano,[29] N. Poljak,[89] A. Pop,[45] S. Porteboeuf-Houssais,[125] V. Pozdniakov,[141] I. Y. Pozos,[44] K. K. Pradhan,[47] S. K. Prasad,[4a,4b] S. Prasad,[47] R. Preghenella,[50] F. Prino,[55] C. A. Pruneau,[134] I. Pshenichnov,[140] M. Puccio,[32] S. Pucillo,[24a,24b] Z. Pugelova,[106] S. Qiu,[84] L. Quaglia,[24a,24b] R. E. Quishpe,[114] S. Ragoni,[14] A. Rakotozafindrabe,[128] L. Ramello,[55,130] F. Rami,[127] S. A. R. Ramirez,[44] T. A. Rancien,[73] M. Rasa,[26a,26b] S. S. Räsänen,[43] R. Rath,[50] M. P. Rauch,[20] I. Ravasenga,[84] K. F. Read,[87,120] C. Reckziegel,[112] A. R. Redelbach,[38] K. Redlich,[79,¶] C. A. Reetz,[97] A. Rehman,[20] F. Reidt,[32] H. A. Reme-Ness,[34] Z. Rescakova,[37] K. Reygers,[94] A. Riabov,[140] V. Riabov,[140] R. Ricci,[28a,28b] M. Richter,[19] A. A. Riedel,[95] W. Riegler,[32] C. Ristea,[62] M. V. Rodriguez,[32] M. Rodríguez Cahuantzi,[44] K. Røed,[19] R. Rogalev,[140] E. Rogochaya,[141] T. S. Rogoschinski,[63] D. Rohr,[32] D. Röhrich,[20] P. F. Rojas,[44] S. Rojas Torres,[35] P. S. Rokita,[133] G. Romanenko,[141] F. Ronchetti,[48] A. Rosano,[30,52] E. D. Rosas,[64] K. Roslon,[133] A. Rossi,[53] A. Roy,[47] S. Roy,[46] N. Rubini,[25a,25b] O. V. Rueda,[114] D. Ruggiano,[133] R. Rui,[23a,23b] P. G. Russek,[2] R. Russo,[84] A. Rustamov,[81] E. Ryabinkin,[140] Y. Ryabov,[140] A. Rybicki,[107] H. Rytkonen,[115] J. Ryu,[16] W. Rzesa,[133] O. A. M. Saarimaki,[43] R. Sadek,[103] S. Sadhu,[31a,31b] S. Sadovsky,[140] J. Saetre,[20] K. Šafařík,[35] P. Saha,[41] S. K. Saha,[4a,4b] S. Saha,[80] B. Sahoo,[46] B. Sahoo,[47] R. Sahoo,[47] S. Sahoo,[60] D. Sahu,[47] P. K. Sahu,[60] J. Saini,[132] K. Sajdakova,[37] S. Sakai,[123] M. P. Salvan,[97] S. Sambyal,[91] I. Sanna,[32,95] T. B. Saramela,[110] D. Sarkar,[134] N. Sarkar,[132] P. Sarma,[41] V. Sarritzu,[22a,22b] V. M. Sarti,[95] M. H. P. Sas,[137] J. Schambach,[87] H. S. Scheid,[63] C. Schiaua,[45] R. Schicker,[94] A. Schmah,[94] C. Schmidt,[97] H. R. Schmidt,[93] M. O. Schmidt,[32] M. Schmidt,[93] N. V. Schmidt,[87] A. R. Schmier,[120] R. Schotter,[127] A. Schröter,[38] J. Schukraft,[32] K. Schwarz,[97] K. Schweda,[97] G. Scioli,[25a,25b] E. Scomparin,[55] J. E. Seger,[14] Y. Sekiguchi,[122] D. Sekihata,[122] I. Selyuzhenkov,[97] S. Senyukov,[127] J. J. Seo,[57] D. Serebryakov,[140] L. Šerkšnytė,[95] A. Sevcenco,[62] T. J. Shaba,[67] A. Shabetai,[103] R. Shahoyan,[32] A. Shangaraev,[140] A. Sharma,[90] B. Sharma,[91] D. Sharma,[46] H. Sharma,[53,107] M. Sharma,[91] S. Sharma,[76] S. Sharma,[91] U. Sharma,[91] A. Shatat,[72] O. Sheibani,[114] K. Shigaki,[92] M. Shimomura,[77] J. Shin,[11] S. Shirinkin,[140] Q. Shou,[39] Y. Sibiriak,[140] S. Siddhanta,[51] T. Siemiarczuk,[79] T. F. Silva,[110] D. Silvermyr,[75] T. Simantathammakul,[105] R. Simeonov,[36] B. Singh,[91] B. Singh,[95] K. Singh,[47] R. Singh,[80] R. Singh,[91] R. Singh,[47] S. Singh,[15] V. K. Singh,[132] V. Singhal,[132] T. Sinha,[99] B. Sitar,[12] M. Sitta,[55,130] T. B. Skaali,[19] G. Skorodumovs,[94] M. Slupecki,[43] N. Smirnov,[137] R. J. M. Snellings,[58] E. H. Solheim,[19] J. Song,[114] A. Songmoolnak,[105] C. Sonnabend,[32,97] F. Soramel,[27a,27b] A. B. Soto-hernandez,[88] R. Spijkers,[84] I. Sputowska,[107] J. Staa,[75] J. Stachel,[94] I. Stan,[62] P. J. Steffanic,[120] S. F. Stiefelmaier,[94] D. Stocco,[103] I. Storehaug,[19] P. Stratmann,[135] S. Strazzi,[25a,25b] C. P. Stylianidis,[84] A. A. P. Suaide,[110] C. Suire,[72] M. Sukhanov,[140] M. Suljic,[32] R. Sultanov,[140] V. Sumberia,[91] S. Sumowidagdo,[82] S. Swain,[60] I. Szarka,[12] M. Szymkowski,[133] S. F. Taghavi,[95] G. Taillepied,[97] J. Takahashi,[111] G. J. Tambave,[80] S. Tang,[6] Z. Tang,[118] J. D. Tapia Takaki,[116] N. Tapus,[124] L. A. Tarasovicova,[135] M. G. Tarzila,[45] G. F. Tassielli,[31a,31b] A. Tauro,[32] G. Tejeda Muñoz,[44] A. Telesca,[32] L. Terlizzi,[24a,24b] C. Terrevoli,[114] S. Thakur,[4a,4b] D. Thomas,[108] A. Tikhonov,[140] A. R. Timmins,[114] M. Tkacik,[106] T. Tkacik,[106] A. Toia,[63] R. Tokumoto,[92] N. Topilskaya,[140] M. Toppi,[48] T. Tork,[72] A. G. Torres Ramos,[31a,31b] A. Trifiró,[30,52] A. S. Triolo,[30,32,52] S. Tripathy,[50] T. Tripathy,[46] S. Trogolo,[32] V. Trubnikov,[3] W. H. Trzaska,[115] T. P. Trzcinski,[133] A. Tumkin,[140] R. Turrisi,[53] T. S. Tveter,[19] K. Ullaland,[20] B. Ulukutlu,[95] A. Uras,[126] M. Urioni,[54,131] G. L. Usai,[22a,22b] M. Vala,[37] N. Valle,[21] L. V. R. van Doremalen,[58] M. van Leeuwen,[84] C. A. van Veen,[94] R. J. G. van Weelden,[84] P. Vande Vyvre,[32] D. Varga,[136] Z. Varga,[136] M. Vasileiou,[78] A. Vasiliev,[140] O. Vázquez Doce,[48] V. Vechernin,[140] E. Vercellin,[24a,24b] S. Vergara Limón,[44] L. Vermunt,[97] R. Vértesi,[136] M. Verweij,[58] L. Vickovic,[33] Z. Vilakazi,[121] O. Villalobos Baillie,[100] A. Villani,[23a,23b] G. Vino,[49] A. Vinogradov,[140] T. Virgili,[28a,28b] M. M. O. Virta,[115] V. Vislavicius,[75] A. Vodopyanov,[141] B. Volkel,[32] M. A. Völkl,[94] K. Voloshin,[140] S. A. Voloshin,[134] G. Volpe,[31a,31b] B. von Haller,[32] I. Vorobyev,[95] N. Vozniuk,[140] J. Vrláková,[37] J. Wan,[39] C. Wang,[39] D. Wang,[39] Y. Wang,[39] A. Wegrzynek,[32] F. T. Weiglhofer,[38] S. C. Wenzel,[32] J. P. Wessels,[135] S. L. Weyhmiller,[137] J. Wiechula,[63] J. Wikne,[19] G. Wilk,[79] J. Wilkinson,[97] G. A. Willems,[135] B. Windelband,[94] M. Winn,[128] J. R. Wright,[108] W. Wu,[39] Y. Wu,[118] R. Xu,[6] A. Yadav,[42] A. K. Yadav,[132] S. Yalcin,[71] Y. Yamaguchi,[92] S. Yang,[20] S. Yano,[92] Z. Yin,[6] I.-K. Yoo,[16] J. H. Yoon,[57] H. Yu,[11] S. Yuan,[20] A. Yuncu,[94] V. Zaccolo,[23a,23b] C. Zampolli,[32] F. Zanone,[94] N. Zardoshti,[32] A. Zarochentsev,[140] P. Závada,[61] N. Zaviyalov,[140]

M. Zhalov,[140] B. Zhang,[6] L. Zhang,[39] S. Zhang,[39] X. Zhang,[6] Y. Zhang,[118] Z. Zhang,[6] M. Zhao,[10] V. Zherebchevskii,[140] Y. Zhi,[10] D. Zhou,[6] Y. Zhou,[83] J. Zhu,[6,97] Y. Zhu,[6] S. C. Zugravel,[55] and N. Zurlo[54,131]

(ALICE Collaboration)

[1]*A. I. Alikhanyan National Science Laboratory (Yerevan Physics Institute) Foundation, Yerevan, Armenia*
[2]*AGH University of Science and Technology, Cracow, Poland*
[3]*Bogolyubov Institute for Theoretical Physics, National Academy of Sciences of Ukraine, Kiev, Ukraine*
[4a]*Bose Institute, Department of Physics, Kolkata, India*
[4b]*Centre for Astroparticle Physics and Space Science (CAPSS), Kolkata, India*
[5]*California Polytechnic State University, San Luis Obispo, California, USA*
[6]*Central China Normal University, Wuhan, China*
[7]*Centro de Aplicaciones Tecnológicas y Desarrollo Nuclear (CEADEN), Havana, Cuba*
[8]*Centro de Investigación y de Estudios Avanzados (CINVESTAV), Mexico City and Mérida, Mexico*
[9]*Chicago State University, Chicago, Illinois, USA*
[10]*China Institute of Atomic Energy, Beijing, China*
[11]*Chungbuk National University, Cheongju, Republic of Korea*
[12]*Comenius University Bratislava, Faculty of Mathematics, Physics and Informatics, Bratislava, Slovak Republic*
[13]*COMSATS University Islamabad, Islamabad, Pakistan*
[14]*Creighton University, Omaha, Nebraska, USA*
[15]*Department of Physics, Aligarh Muslim University, Aligarh, India*
[16]*Department of Physics, Pusan National University, Pusan, Republic of Korea*
[17]*Department of Physics, Sejong University, Seoul, Republic of Korea*
[18]*Department of Physics, University of California, Berkeley, California, USA*
[19]*Department of Physics, University of Oslo, Oslo, Norway*
[20]*Department of Physics and Technology, University of Bergen, Bergen, Norway*
[21]*Dipartimento di Fisica, Università di Pavia, Pavia, Italy*
[22a]*Dipartimento di Fisica dell'Università, Cagliari, Italy*
[22b]*Sezione INFN, Cagliari, Italy*
[23a]*Dipartimento di Fisica dell'Università, Trieste, Italy*
[23b]*Sezione INFN, Trieste, Italy*
[24a]*Dipartimento di Fisica dell'Università, Turin, Italy*
[24b]*Sezione INFN, Turin, Italy*
[25a]*Dipartimento di Fisica e Astronomia dell'Università, Bologna, Italy*
[25b]*Sezione INFN, Bologna, Italy*
[26a]*Dipartimento di Fisica e Astronomia dell'Università, Catania, Italy*
[26b]*Sezione INFN, Catania, Italy*
[27a]*Dipartimento di Fisica e Astronomia dell'Università, Padova, Italy*
[27b]*Sezione INFN, Padova, Italy*
[28a]*Dipartimento di Fisica 'E.R. Caianiello' dell'Università, Salerno, Italy*
[28b]*Gruppo Collegato INFN, Salerno, Italy*
[29]*Dipartimento DISAT del Politecnico and Sezione INFN, Turin, Italy*
[30]*Dipartimento di Scienze MIFT, Università di Messina, Messina, Italy*
[31a]*Dipartimento Interateneo di Fisica 'M. Merlin', Bari, Italy*
[31b]*Sezione INFN, Bari, Italy*
[32]*European Organization for Nuclear Research (CERN), Geneva, Switzerland*
[33]*Faculty of Electrical Engineering, Mechanical Engineering and Naval Architecture, University of Split, Split, Croatia*
[34]*Faculty of Engineering and Science, Western Norway University of Applied Sciences, Bergen, Norway*
[35]*Faculty of Nuclear Sciences and Physical Engineering, Czech Technical University in Prague, Prague, Czech Republic*
[36]*Faculty of Physics, Sofia University, Sofia, Bulgaria*
[37]*Faculty of Science, P.J. Šafárik University, Košice, Slovak Republic*
[38]*Frankfurt Institute for Advanced Studies, Johann Wolfgang Goethe-Universität Frankfurt, Frankfurt, Germany*
[39]*Fudan University, Shanghai, China*
[40]*Gangneung-Wonju National University, Gangneung, Republic of Korea*
[41]*Gauhati University, Department of Physics, Guwahati, India*

[42]*Helmholtz-Institut für Strahlen- und Kernphysik, Rheinische Friedrich-Wilhelms-Universität Bonn, Bonn, Germany*
[43]*Helsinki Institute of Physics (HIP), Helsinki, Finland*
[44]*High Energy Physics Group, Universidad Autónoma de Puebla, Puebla, Mexico*
[45]*Horia Hulubei National Institute of Physics and Nuclear Engineering, Bucharest, Romania*
[46]*Indian Institute of Technology Bombay (IIT), Mumbai, India*
[47]*Indian Institute of Technology Indore, Indore, India*
[48]*INFN, Laboratori Nazionali di Frascati, Frascati, Italy*
[49]*INFN, Sezione di Bari, Bari, Italy*
[50]*INFN, Sezione di Bologna, Bologna, Italy*
[51]*INFN, Sezione di Cagliari, Cagliari, Italy*
[52]*INFN, Sezione di Catania, Catania, Italy*
[53]*INFN, Sezione di Padova, Padova, Italy*
[54]*INFN, Sezione di Pavia, Pavia, Italy*
[55]*INFN, Sezione di Torino, Turin, Italy*
[56]*INFN, Sezione di Trieste, Trieste, Italy*
[57]*Inha University, Incheon, Republic of Korea*
[58]*Institute for Gravitational and Subatomic Physics (GRASP), Utrecht University/Nikhef, Utrecht, Netherlands*
[59]*Institute of Experimental Physics, Slovak Academy of Sciences, Košice, Slovak Republic*
[60]*Institute of Physics, Homi Bhabha National Institute, Bhubaneswar, India*
[61]*Institute of Physics of the Czech Academy of Sciences, Prague, Czech Republic*
[62]*Institute of Space Science (ISS), Bucharest, Romania*
[63]*Institut für Kernphysik, Johann Wolfgang Goethe-Universität Frankfurt, Frankfurt, Germany*
[64]*Instituto de Ciencias Nucleares, Universidad Nacional Autónoma de México, Mexico City, Mexico*
[65]*Instituto de Física, Universidade Federal do Rio Grande do Sul (UFRGS), Porto Alegre, Brazil*
[66]*Instituto de Física, Universidad Nacional Autónoma de México, Mexico City, Mexico*
[67]*iThemba LABS, National Research Foundation, Somerset West, South Africa*
[68]*Jeonbuk National University, Jeonju, Republic of Korea*
[69]*Johann-Wolfgang-Goethe Universität Frankfurt Institut für Informatik, Fachbereich Informatik und Mathematik, Frankfurt, Germany*
[70]*Korea Institute of Science and Technology Information, Daejeon, Republic of Korea*
[71]*KTO Karatay University, Konya, Turkey*
[72]*Laboratoire de Physique des 2 Infinis, Irène Joliot-Curie, Orsay, France*
[73]*Laboratoire de Physique Subatomique et de Cosmologie, Université Grenoble-Alpes, CNRS-IN2P3, Grenoble, France*
[74]*Lawrence Berkeley National Laboratory, Berkeley, California, USA*
[75]*Division of Particle Physics, Lund University, Department of Physics, Lund, Sweden*
[76]*Nagasaki Institute of Applied Science, Nagasaki, Japan*
[77]*Nara Women's University (NWU), Nara, Japan*
[78]*Department of Physics, National and Kapodistrian University of Athens, School of Science, Athens, Greece*
[79]*National Centre for Nuclear Research, Warsaw, Poland*
[80]*National Institute of Science Education and Research, Homi Bhabha National Institute, Jatni, India*
[81]*National Nuclear Research Center, Baku, Azerbaijan*
[82]*National Research and Innovation Agency—BRIN, Jakarta, Indonesia*
[83]*Niels Bohr Institute, University of Copenhagen, Copenhagen, Denmark*
[84]*Nikhef, National Institute for Subatomic Physics, Amsterdam, Netherlands*
[85]*Nuclear Physics Group, STFC Daresbury Laboratory, Daresbury, United Kingdom*
[86]*Nuclear Physics Institute of the Czech Academy of Sciences, Husinec-Řež, Czech Republic*
[87]*Oak Ridge National Laboratory, Oak Ridge, Tennessee, USA*
[88]*Ohio State University, Columbus, Ohio, USA*
[89]*Physics Department, Faculty of Science, University of Zagreb, Zagreb, Croatia*
[90]*Physics Department, Panjab University, Chandigarh, India*
[91]*Physics Department, University of Jammu, Jammu, India*
[92]*Physics Program and International Institute for Sustainability with Knotted Chiral Meta Matter (SKCM2), Hiroshima University, Hiroshima, Japan*
[93]*Physikalisches Institut, Eberhard-Karls-Universität Tübingen, Tübingen, Germany*
[94]*Physikalisches Institut, Ruprecht-Karls-Universität Heidelberg, Heidelberg, Germany*
[95]*Physik Department, Technische Universität München, Munich, Germany*

[96]*Politecnico di Bari and Sezione INFN, Bari, Italy*
[97]*Research Division and ExtreMe Matter Institute EMMI, GSI Helmholtzzentrum für Schwerionenforschung GmbH, Darmstadt, Germany*
[98]*Saga University, Saga, Japan*
[99]*Saha Institute of Nuclear Physics, Homi Bhabha National Institute, Kolkata, India*
[100]*School of Physics and Astronomy, University of Birmingham, Birmingham, United Kingdom*
[101]*Sección Física, Departamento de Ciencias, Pontificia Universidad Católica del Perú, Lima, Peru*
[102]*Stefan Meyer Institut für Subatomare Physik (SMI), Vienna, Austria*
[103]*SUBATECH, IMT Atlantique, Nantes Université, CNRS-IN2P3, Nantes, France*
[104]*Sungkyunkwan University, Suwon City, Republic of Korea*
[105]*Suranaree University of Technology, Nakhon Ratchasima, Thailand*
[106]*Technical University of Košice, Košice, Slovak Republic*
[107]*The Henryk Niewodniczanski Institute of Nuclear Physics, Polish Academy of Sciences, Cracow, Poland*
[108]*The University of Texas at Austin, Austin, Texas, USA*
[109]*Universidad Autónoma de Sinaloa, Culiacán, Mexico*
[110]*Universidade de São Paulo (USP), São Paulo, Brazil*
[111]*Universidade Estadual de Campinas (UNICAMP), Campinas, Brazil*
[112]*Universidade Federal do ABC, Santo Andre, Brazil*
[113]*University of Cape Town, Cape Town, South Africa*
[114]*University of Houston, Houston, Texas, USA*
[115]*University of Jyväskylä, Jyväskylä, Finland*
[116]*University of Kansas, Lawrence, Kansas, USA*
[117]*University of Liverpool, Liverpool, United Kingdom*
[118]*University of Science and Technology of China, Hefei, China*
[119]*University of South-Eastern Norway, Kongsberg, Norway*
[120]*University of Tennessee, Knoxville, Tennessee, USA*
[121]*University of the Witwatersrand, Johannesburg, South Africa*
[122]*University of Tokyo, Tokyo, Japan*
[123]*University of Tsukuba, Tsukuba, Japan*
[124]*University Politehnica of Bucharest, Bucharest, Romania*
[125]*Université Clermont Auvergne, CNRS/IN2P3, LPC, Clermont-Ferrand, France*
[126]*Université de Lyon, CNRS/IN2P3, Institut de Physique des 2 Infinis de Lyon, Lyon, France*
[127]*Université de Strasbourg, CNRS, IPHC UMR 7178, F-67000 Strasbourg, France, Strasbourg, France*
[128]*Université Paris-Saclay Centre d'Etudes de Saclay (CEA), IRFU, Départment de Physique Nucléaire (DPhN), Saclay, France*
[129]*Università degli Studi di Foggia, Foggia, Italy*
[130]*Università del Piemonte Orientale, Vercelli, Italy*
[131]*Università di Brescia, Brescia, Italy*
[132]*Variable Energy Cyclotron Centre, Homi Bhabha National Institute, Kolkata, India*
[133]*Warsaw University of Technology, Warsaw, Poland*
[134]*Wayne State University, Detroit, Michigan, USA*
[135]*Westfälische Wilhelms-Universität Münster, Institut für Kernphysik, Münster, Germany*
[136]*Wigner Research Centre for Physics, Budapest, Hungary*
[137]*Yale University, New Haven, Connecticut, USA*
[138]*Yonsei University, Seoul, Republic of Korea*
[139]*Zentrum für Technologie und Transfer (ZTT), Worms, Germany*
[140]*Affiliated with an institute covered by a cooperation agreement with CERN*
[141]*Affiliated with an international laboratory covered by a cooperation agreement with CERN*

[†]Deceased.
[‡]Also at Max-Planck-Institut für Physik, Munich, Germany.
[§]Also at Italian National Agency for New Technologies, Energy and Sustainable Economic Development (ENEA), Bologna, Italy.
[‖]Also at Department of Applied Physics, Aligarh Muslim University, Aligarh, India.
[¶]Also at Institute of Theoretical Physics, University of Wroclaw, Poland.
[**]Also at an institution covered by a cooperation agreement with CERN.